



An ignition delay time and chemical kinetic modeling study of the pentane isomers

Title	An ignition delay time and chemical kinetic modeling study of the pentane isomers
Author(s)	Bugler, John;Heufer, Karl A.;Curran, Henry J.
Publication Date	2016-10-26
Publisher	Elsevier
Repository DOI	10.1016/j.combustflame.2015.09.014

Title Page

An Ignition Delay Time and Chemical Kinetic Modelling Study of the Pentane Isomers

John Bugler^a, Brandon Marks^b, Olivier Mathieu^b, Rachel Archuleta^b, Alejandro Camou^b, Claire Grégoire^b, Karl A. Heufer^a, Eric L. Petersen^b, Henry J. Curran^a

^aCombustion Chemistry Centre, National University of Ireland, Galway, Ireland

^bTexas A&M University, College Station, TX, USA

Corresponding author:

Prof. Henry J. Curran,

Combustion Chemistry Centre,

National University of Ireland, Galway

Ireland.

Email address:

henry.curran@nuigalway.ie

Type of article: full-length

An Ignition Delay Time and Chemical Kinetic Modeling Study of the Pentane Isomers

John Bugler^a, Brandon Marks^b, Olivier Mathieu^b, Rachel Archuleta^b, Alejandro Camou^b, Claire Grégoire^b, Karl A. Heufer^a, Eric L. Petersen^b, Henry J. Curran^{a,*}

^aCombustion Chemistry Centre, National University of Ireland, Galway, Ireland

^bTexas A&M University, College Station, TX, USA

Abstract

Ignition delay times of *n*-pentane, *iso*-pentane, and *neo*-pentane mixtures were measured in two shock tubes and in a rapid compression machine. The experimental data were used as validation targets for the model described in detail in an accompanying study [J. Bugler, K. P. Somers, E. J. Silke, H. J. Curran, Revisiting the Kinetics and Thermodynamics of the Low-Temperature Oxidation Pathways of Alkanes: A Case Study of the Three Pentane Isomers, *J. Phys. Chem. A* 119 (28) (2015) 7510–7527]. The present study presents ignition delay time data for the pentane isomers at equivalence ratios of 0.5, 1.0, and 2.0 in ‘air’ (additionally, 0.3 in ‘air’ for *n*-, and *iso*-pentane) at pressures of 1, 10, and 20 atm in the shock tube, and 10 and 20 atm in the rapid compression machine, as well as data at an equivalence ratio of 1.0 in 99% argon, at pressures near 1 and 10 atm in a shock tube. An infrared laser absorption technique at 3.39 μm was used to verify the composition of the richest mixtures in the shock-tube tests by measuring directly the pentane isomer concentration in the driven section. By using shock tubes and a rapid compression machine, it was possible to investigate temperatures ranging from 643–1718 K. A detailed chemical kinetic model was used to simulate the experimental ignition delay times, and these are well-predicted for all of the isomers over all ranges of temperature, pressure, and mixture composition. In-depth analyses, including reaction path and sensitivity analyses, of the oxidation mechanisms of each of the isomers are presented. To the authors’ knowledge, this study covers conditions not yet presented in the literature and will, in conjunction with the aforementioned accompanying study, expand fundamental knowledge of the combustion kinetics of the pentane isomers and alkanes in general.

Keywords: shock tube; rapid compression machine; kinetic modeling; alkane; pentane

1. Introduction

The combustion and chemical kinetics of *n*-pentane are of interest because it is a component of gas-turbine and gasoline engine fuel blends and is an intermediate species in the oxidation of higher-order hydrocarbons. For this reason, several studies have investigated its combustion characteristics and mechanism of oxidation. Literature data are scarcer concerning *iso*- and *neo*-pentane. While models for straight-chained alkanes have matured for species relevant to transportation fuels, much less work has been performed on branched alkanes, which are a large component in petrol and diesel fuels. Ignition delay time (IDT) data are particularly useful in the validation of kinetic mechanisms, and this study aims to increase the fidelity of the pentane isomer models utilizing these data. Several studies have been performed that examined the combustion of the pentane isomers, which include rapid compression machines (RCM) [1–4], shock tubes (ST) [5–7], a well-stirred reactor [8], and an annular flow reactor study [9].

* henry.curran@nuigalway.ie

Combustion Chemistry Centre, National University of Ireland, Galway, Ireland

Dahm and Verhoek [5] explored the gas-phase oxidation of *n*-pentane in the low-temperature region, 595–732 K. A study by Burcat and co-workers [6] compared the IDTs of C₁–C₅ alkanes at stoichiometric conditions utilizing a shock tube at pressures between 8.27 and 9.46 atm over a temperature range of 1165–1400 K. Gonzalez and Sandler used an annular flow reactor to study the oxidation of an *n*-pentane/air mixture in the high-temperature, pre-ignition region in the temperature range of 773–893 K [9]. Westbrook *et al.* studied the oxidation of *n*-pentane at 1 atm and at temperatures ranging from 1068–1253 K using a well-stirred reactor [8]. Three RCM studies were published by Minetti *et al.* [3,4] and Westbrook *et al.* [1]. Minetti and co-workers studied the autoignition of alkanes in the intermediate temperature range from 630–920 K at equivalence ratios between 0.8 and 1.2, and at pressures between 3 and 16 bar, and concluded that the data were in relatively good agreement with the mechanism predictions. Minetti *et al.* also compared the pre-ignition chemistry of *n*-pentane and 1-pentene under stoichiometric conditions at pressures between 6.8 and 9.2 bar and at temperatures from 600–900 K. Autoignition, kinetic reaction mechanisms, and model agreement were studied by Westbrook *et al.* for equivalence ratios between 0.5 and 2.0, at pressures from 8–20 bar, and temperatures from 675–980 K. Excellent agreement between computed and measured results was found [1]. An RCM study conducted by Ribaucour *et al.* compared the three isomers of pentane at stoichiometric conditions at initial pressures of 300 and 400 Torr and at temperatures ranging from 640–900 K [2]. A high-pressure shock tube study was performed by Zhukov *et al.* in which lean *n*-pentane IDTs were measured to aid development of a kinetic model [7]. Tests were performed at an equivalence ratio of 0.5 and over pressure and temperature ranges of 11–530 atm and 867–1534 K, respectively. It was concluded that the kinetic model was in good agreement with experimental data obtained therein. Oehlschlaeger *et al.* used a shock tube to measure IDTs of *iso*-pentane at equivalence ratios from 0.25–2.0 at pressures ranging from 1.10–12.58 atm and temperatures ranging from 1177–2009 K [10]. A flow reactor study of *neo*-pentane was carried out at a pressure of 8 atm, at an equivalence ratio of 0.3 and at temperatures ranging from 620–810 K by Wang *et al.* [11].

This study adds to the literature by extending the range of conditions for each of the fuels, most notably for *iso*- and *neo*-pentane for which there have been few experimental studies compared to *n*-pentane. However, this study represents more than simply extending a matrix of experimental conditions. The three isomers, although relatively small, exhibit significant structural diversity, and are the smallest isomeric set of alkanes containing linear, singly-branched, and doubly-branched species. Knowing the effects that these structural differences have on the reactivity of the fuels is of importance, especially for typical transportation fuels which contain a large amount of alkanes with various amounts of structural branching. Also, between the isomers there should be adequate structural variation to be representative of all larger alkanes. An example is observed in the similarity between *iso*- and *neo*-pentane and the varyingly branched portions of *iso*-octane. *n*-Pentane may also be an ideal analogue for larger normal alkanes due to the proximity of its outermost secondary carbons. The relatively fast isomerization reactions of alkyl-peroxyl and hydroperoxyl-alkyl-peroxyl radicals via 6-membered transition state rings can occur between these two secondary carbons. This is the smallest normal alkane for which this fast isomerization can occur, and it is the dominant kind of pathway for larger alkanes at low temperatures (600–900 K). This makes it a better archetype for low-temperature alkane oxidation chemistry than propane or *n*-butane, for example, neither of which have a long enough alkyl chain to be truly representative of longer normal alkanes.

As well as being representative of larger highly branched alkyl structures, *neo*-pentane itself shows interesting characteristics. It is the smallest alkane that contains only primary and quaternary carbons, with the next smallest alkane of this type being *neo*-octane (2,2,3,3-tetramethylbutane). As discussed in Section 3.3, this uncommon structure results in the lack of a major uni-molecular pathway of the alkyl-peroxy radical, which is present for all but the *neo*-alkanes. This causes *neo*-pentane to show abnormal trends in reactivity as a function of temperature. Its highly symmetric nature also means that the amount of different types of species and reactions involved in its oxidation pathways is greatly reduced compared to its isomers. In terms of kinetic modeling, this introduces an extra layer of constraint on model parameters, due to there being far less possible combinations of input values. This helps ensure that a situation does not occur in which a series of compensating errors in thermochemical and reaction rate assignments can approximate accurate predictions for a given set of validation targets.

In this study, data were collected experimentally using shock tubes and an RCM at elevated pressures and temperatures, as presented below. The proposed model is presented in comparison to the data for validation. Provided first are details of the experiments, followed by a presentation of the extensive results and corresponding discussion. Comparisons with the chemical kinetic model are provided in the same plots with the experimental data.

2. Experimental

Fuel/‘air’ mixtures were studied for *n*- and *iso*-pentane at equivalence ratios of 0.3, 0.5, 1.0, and 2.0, and at equivalence ratios of 0.5, 1.0, and 2.0 for *neo*-pentane. ‘Air’ in the case of the experiments presented in this study refers to nitrogen (or argon/carbon dioxide) and oxygen in a 79-to-21 ratio, respectively. New data are also presented for each of the isomers at stoichiometric, highly dilute (99% argon) conditions at pressures near 1 and 10 atm. Experiments were performed at pressures near 1, 10, and 20 atm, and at temperatures ranging from 778 to 1718 K in the shock tubes, and at 10 and 20 atm in the RCM at temperatures between 643 and 1065 K. The ST experiments were carried out in the high pressure ST at Texas A&M University (TAMU) and the high pressure ST at NUI Galway’s (NUIG) Combustion Chemistry Centre. All RCM experiments were carried out in one of the twin-opposed piston RCMs at NUIG. Experimental data were used to make improvements to the chemical kinetic mechanisms previously developed by Healy *et al.*, Curran *et al.* and Wang *et al* [11–13], as detailed in the partner study to this one [14]. Mixtures were composed of spectrophotometer grade ($\geq 99\%$) *n*-pentane, *iso*-pentane, and *neo*-pentane; and high purity ($\geq 99.5\%$) oxygen and nitrogen. Experimental conditions investigated in this study are outlined in Table 1. Ignition delay times reported in this study along with associated pressure and temperature conditions are available in Supplementary material, as well as plots of model performance against other literature targets.

Table 1. Experimental conditions studied here in shock tubes and an RCM.

Fuel	T (K)	p (atm)	ϕ	dilution
<i>n</i> -C ₅ H ₁₂	643–1555	1–20	0.3–2.0	~75–99%
<i>iso</i> -C ₅ H ₁₂	663–1675	1–20	0.3–2.0	~75–99%
<i>neo</i> -C ₅ H ₁₂	651–1718	1–20	0.5–2.0	~75–99%

2.1. TAMU Shock Tube Hardware

The shock tube is constructed of 304 stainless steel. The driven section is 4.72 m in length, and the driver section is 2.46 m long. The shock-tube diameter is 15.24 cm, and the inner surface is polished to 1 micron RMS to reduce boundary layer formation. Five PCB 113 pressure transducers along the driven section of the tube are used to measure the incident-shock velocity. The pressure transducer signal is fed to four Fluke PM 6666 timer counter boxes to measure the time it takes the shock to pass from one transducer to the next. The time intervals are then extrapolated to find the incident-shock velocity at the endwall. As a result, the experimental reflected-shock temperature is known to within 15 K. Helium was used as the driving gas throughout. For the 1 and 10 atm experiments, polycarbonate diaphragms were used to separate the driving gas from the test mixture, and scored aluminum diaphragms were used for the 20 atm experiments. All experiments were performed behind the reflected shock wave. Small viewing ports adjacent to the endwall allow for the capture of light emission during combustion. More details on the shock tube are available in Aul et al. [15].

A mixing tank was evacuated to less than 5×10^{-5} Torr and filled to the proper species concentration using the partial pressures method. Gases were passed through a perforated stinger traversing the center of the mixing tank to allow for rapid, turbulent mixing. At least 24 hours was allowed to pass between the creation of the mixture and experimental runs, to allow for complete homogeneous mixing of the gases.

During the preparation of large fuel-rich mixtures, some fuel condensation was observed. To minimize this condensation, mixtures were prepared in smaller batches, and the validity of the mixture preparation method at these conditions was cross-checked by direct measurement of the fuel concentration in the shock tube using a laser absorption technique. Mid-IR lasers have been used to measure hydrocarbons due to their strong absorption bands near 3.4 μm caused by C-H bonds. These strong absorption bands are coincident with a helium-neon laser (He-Ne) that operates at 3.39 μm .

The gas concentration can be computed by relating the optical, geometrical, and spectroscopic parameters using the Beer-Lambert relation. The Beer-Lambert relation describes the laser intensity attenuation as a beam of light from a monochromatic source is transmitted through a gas sample of length L per the following well-known relation:

$$\left(\frac{I_t}{I_o} \right)_v = \exp(-L \cdot \sigma_v \cdot C_{Fuel}) \quad (1)$$

Where I_t and I_o represent the transmitted and incident laser intensity, respectively; σ_v is the absorption cross section [m^2/mole] at frequency v ; L is the sample path length [m]; and C_{Fuel} [mole/m^3] is the concentration of the targeted hydrocarbon fuel. The fuel concentration can be calculated by rearranging Eq. (1) and comparing it to the ideal gas relation as shown below.

$$C_{Fuel} = \frac{-\ln\left(\frac{I_t}{I_o}\right)}{L \cdot \sigma_v} = \frac{X_{Fuel} \cdot P_{Total}}{R \cdot T} \quad (2)$$

From the above relation, X_{Fuel} is the fuel mole fraction, P_{Total} is the total pressure of the mixture, R is the universal gas constant, and T is the temperature of the mixture. Equation (2) can be used to

validate the fuel concentration measured via laser diagnostics. The absorption cross section is species-specific and can also be temperature and pressure dependent. Extensive studies have been made to investigate the effects of temperature and pressure on the absorption cross section for various hydrocarbons. Mével et al. [16] presented a compilation of several studies of absorption cross section data for alkanes, aromatics, and substituted hydrocarbons at 3.39 μm .

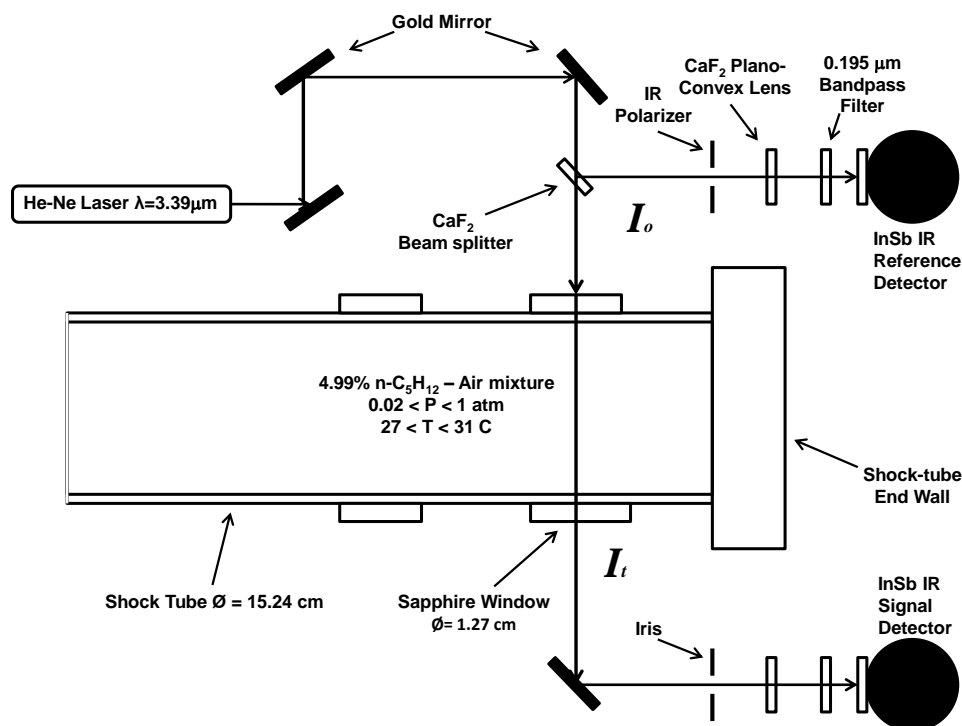


Figure 1. Experimental setup for the measurement of *n*-pentane and *iso*-pentane concentration in the shock tube.

Figure 1 illustrates the laser diagnostic setup using the infrared He-Ne laser. The laser beam passes through a series of gold-coated mirrors followed by a calcium fluoride beam splitter. It is then split into two beams. The reflected beam, which is represented by the incident intensity I_0 after the beam splitter, goes through an IR polarizer to attenuate the beam and prevent detector saturation. The beam then passes through a plano-convex calcium fluoride lens to focus the beam onto the 1 mm-diameter indium antimonide (InSb) reference detector. This InSb reference detector is sealed in a dewar that is cryogenically-cooled using liquid nitrogen. A narrow bandpass filter (0.0195 μm full-width, half maximum) was placed before the detector to block out any unwanted IR radiation. The transmitted beam, I_t , goes through the sapphire window ports of the shock tube and onto the InSb signal detector through a series of optics similar to the reference side. This particular common mode rejection setup allows for correction to minimize any laser power drift as high as 30% from the He-Ne laser due to its sensitivity to ambient conditions, as noted by Klingbeil et al. [17].

As mentioned above, the fuel-rich mixtures were found to be problematic because of potential fuel condensation during the mixture preparation. This likelihood of condensation was even more the case for *n*-pentane, for which the saturated vapor pressure is lower than for *iso*- or *neo*-pentane. The mixture of interest for the direct measurement of the fuel concentration using the laser absorption diagnostic was therefore the *n*-pentane mixture at $\phi = 2.0$: 4.99% $n\text{-C}_5\text{H}_{12}$ / 19.97% O_2 / 75.05% N_2 . The mixture was prepared in a mixing tank following the procedure described earlier. Prior to taking data, the shock tube was evacuated, and the signals from the detectors were balanced to obtain the zero reference condition. The driven section of the shock tube was then filled with the mixture, in the same manner as done for a reflected-shock experiment. The total mixture pressure

for the experiments ranged from 0.02 atm to less than 1 atm. The pressure limit was set to approximately 500 Torr (0.66 atm) due to full attenuation of the laser signal at the corresponding concentration of *n*-pentane. All fill tests were performed at room temperature, which varied from 27–30 °C.

Mével et al. [16] concluded that the absorption cross section of large n-alkanes is independent of temperature in the studied temperature range of 303 to 413 K. The absorption cross section for *n*-pentane in this temperature range varies from 31.75 to 33.5 m²/mol, and the relative uncertainty of the absorption cross section was found to be less than 5%.

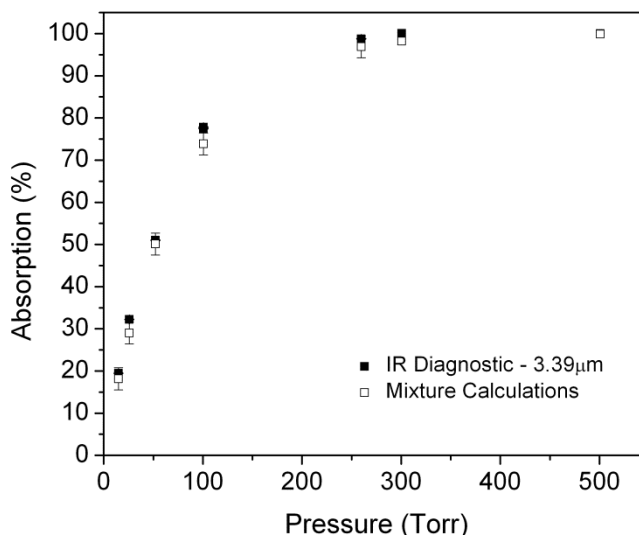


Figure 2. Measured *n*-C₅H₁₂ absorption at 3.39 μm ($X_{n-C_5H_{12}} = 4.99\%$) from the shock tube in comparison to the level calculated from the mixture concentration from the mixing tank.

Figure 2 illustrates the measured absorption percentage of *n*-pentane at room temperature as a function of mixture pressure. The absorption data taken from the laser diagnostic is compared to the absorption level calculated using the ideal gas law, per the mole fraction of the fuel in the mixture directly in the mixing tank. The uncertainty of the mixture calculations is dominated by the absorption cross section uncertainty. Figure 2 shows full attenuation of light at approximately 300 Torr. Figure 3 illustrates the comparison of the calculated *n*-pentane concentration between the absorption diagnostics and the ideal gas law. The fuel concentration uncertainty at 260 Torr is approximately 4%. This larger relative uncertainty may be due to a combination of laser drift after the common mode rejection and an absorption of approximately 98%. The attenuation of light close to 100% reduces the signal-to-noise ratio and causes a higher uncertainty. One can therefore conclude from these direct measurements of the fuel concentration in the shock tube that the careful procedure for the mixture preparation allowed for an accurate mixture composition. That is, Fig. 3 demonstrates that the mole fraction of the fuel in the mixing tank is the same as the fraction of the fuel that makes it to the shock-tube driven section.

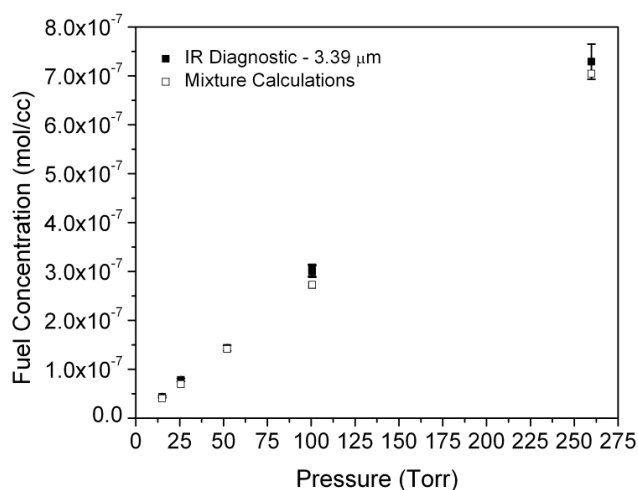


Figure 3. Fuel concentration measurement directly in the shock tube using the 3.39 μm laser diagnostic and the value from the ideal gas relation based on the amount of *n*-pentane in the mixing tank.

Ignition delay time for mixtures in ‘air’ was defined in this study as the time between the arrival of the shock wave at the endwall and the time at which the endwall pressure signal exhibits a sharp increase due to the mixture reactivity, as reported in [15, 18]. Note that this time also corresponds to the intersection of the steepest recorded slope with the baseline of the OH^* emission signal. A representative example of ignition delay time determination from experimental profiles is provided in Fig. 4. As can be seen for this relatively long ignition delay time, at the high-pressure condition, there is no noticeable increase in the pressure before the ignition event. One can also see that the pressure profile calculated with the chemical kinetic model using the constant-volume, constant internal energy ($U-V$) constraint reproduces this pressure profile very well. This agreement between the model and data indicates that there is no significant pressure increase introduced by any facility gas-dynamics related effect.

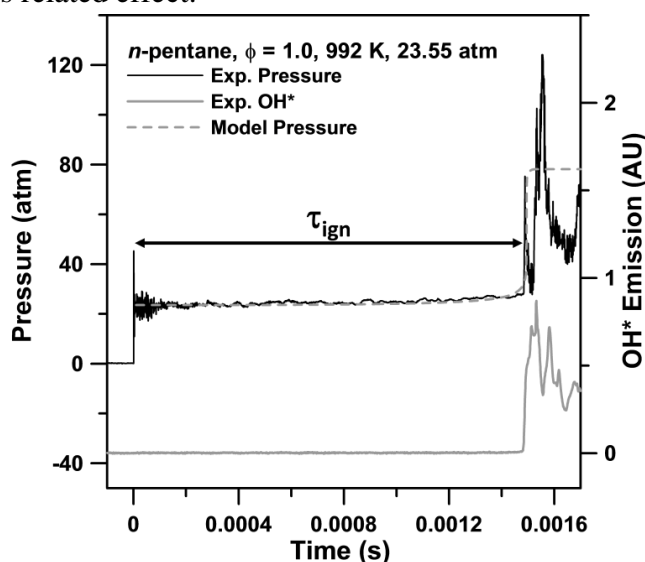


Figure 4. Determination of ignition delay time for mixtures in ‘air’ utilizing endwall pressure and OH^* emission profiles.

For the mixtures diluted in 99% Ar, the ignition delay time corresponds to the time between the passage of the reflected shock wave, indicated by a pressure jump in the signal recorded by the sidewall pressure transducer, and the intersection of lines drawn along the steepest rate-of-change of OH^* de-excitation and a horizontal line which defines the zero-concentration level, as can be seen in Fig. 5.

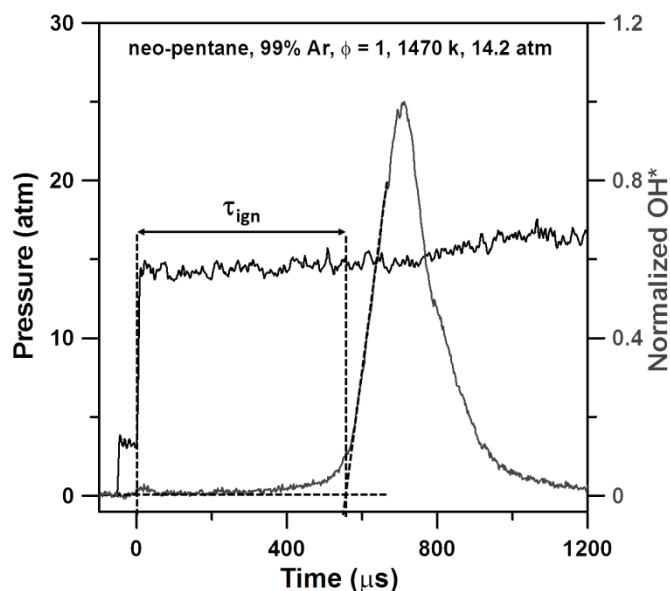


Figure 5. Method of determination of the ignition delay time for the highly diluted mixtures.

2.2. NUIG Shock Tube

The high-pressure shock tube at NUI Galway was used to measure ignition delay times for *n*- and *neo*-pentane at low to intermediate temperatures (~ 750 – 1100 K) at 20 atm, for mixtures where IDTs were too short to be reliably obtainable in the RCM. A brief description of the facility will be given here, as detailed information is presented elsewhere [19].

The 63.5 mm internal diameter tube is separated into three sections: (1) a 5.73 m long driven section where the fuel/‘air’ mixtures to be studied are introduced, (2) a 3 m long driver section where the He or He/N₂ driver gas is loaded, and (3) a 3 cm double-diaphragm section which is located between the driver and driven sections. Two pre-scored aluminium diaphragms are placed in the double-diaphragm section prior to each experiment, and are employed to reach the high pressure reflected shock conditions.

The shock velocity is interpolated at five locations along the driven section by measuring the incident shock arrival times at six axially staggered, sidewall mounted PCB 113B24 pressure transducers. The endwall shock velocity is calculated by linearly extrapolating the five velocities to the endwall. Pressure-time histories at the shock tube endwall are monitored using a Kistler 603B pressure transducer mounted flush with the endwall. Ignition delay times are measured using this endwall pressure transducer, and are taken to be the time between the arrival of the shock wave at the endwall and the ignition event. Well-defined ignition events have been observed for all of the conditions investigated here.

2.3. Rapid Compression Machine

A clone of the original NUIG RCM was used in this study, which is characteristically different to most other RCMs in that it has a twin-opposed piston configuration, as described previously [20], resulting in a fast compression time of approximately 16 ms. In order to improve the post-compression temperature distribution in the combustion chamber, creviced pistons were used [21]. The design for these creviced pistons was originally devised at MIT by Lee and Hochgreb [22,23]. In that study, it was found that the temperature field obtained using creviced pistons is almost homogeneous compared to that obtained using non-creviced pistons. The use of non-creviced

pistons is predicted to lead to far greater gas in-homogeneities in the post-compressed combustion chamber. A computational fluid dynamics (CFD) study carried out by Würmel and Simmie [24] supports this view. Subsequent, in-house CFD calculations were carried out for the piston geometry used for experiments in this study. These piston heads achieve an approximate compression ratio of 12.5:1.

Different compressed gas temperatures are reached by (i) varying the diluent gas used, (typically N₂, Ar, and CO₂ are used) and (ii) using different initial temperatures. Using CO₂ in the diluent mixture allows measurement of IDTs at lower temperatures, while the use of Ar allows higher temperatures to be studied due to its lower heat capacity. The current configuration allowed the majority of RCM experiments in this study to be carried out using 100% N₂ as the bath gas.

Pressure-time profiles are measured using a Kistler 6045A pressure transducer and transferred via a Kistler 5018 amplifier to a Picoscope 4424 oscilloscope, and ultimately recorded digitally on computer using the Picolog PC software. The ignition delay time is measured using two vertical cursors on the oscilloscope, and is defined as the time from the first local maximum in the pressure-time history to the maximum rate of pressure rise due to ignition. The compressed gas pressure was measured using two horizontal cursors.

The initial temperature, T_i , pressure, p_i , reactant composition, and the experimentally measured compressed gas pressure, p_c , were used to calculate the compressed gas temperature, T_c . The adiabatic compression/expansion routine in Gaseq [25] was used for this calculation, which uses the temperature dependence of the ratio of specific heats, γ , according to the equation:

$$\ln\left(\frac{p_c}{p_i}\right) = \int_{T_i}^{T_c} \frac{\gamma}{\gamma - 1} \frac{dT}{T}$$

A frozen chemistry assumption is made for the compression period. The measured ignition delay times are plotted versus the inverse of the compressed gas temperature to obtain overall reactivity profiles of *n*-, *iso*-, and *neo*-pentane.

Heat loss to the chamber walls is assumed to be low during the compression phase, as the time for compression is fast (~16 ms), with most of the rapid rise in pressure and temperature taking place in the last 2–3 ms of compression. More details of the facility can be found in Ref. 26.

To ensure that condensation of the fuels was not occurring, a 3.39 μm He-Ne laser diagnostic setup was utilized. This particular setup has been detailed elsewhere [26], and is quite similar to the one described in Section 2.1, so the description here will be brief. As was tested in the TAMU shock tube, the fuel with the lowest vapor pressure (*n*-pentane) was examined at the most fuel-rich conditions under which experiments were conducted ($\phi = 2.0$ in ‘air’). No evidence of condensation was observed at these conditions.

The gases experience heat loss for a period following compression due to the high temperature of the gas within the chamber relative to the chamber walls. The core gas continues to lose heat during the constant volume period, and therefore simulation of the experiments cannot be performed under adiabatic, constant volume conditions, even though the geometric volume is not varying with time. In order to model the experiments, a non-reactive experiment is performed for every reactive

condition. The non-reactive mixture composition is the same as that of the reactive mixture except that O₂ is replaced by an equivalent amount of N₂, as molecular nitrogen is unreactive and has similar thermodynamic properties to molecular oxygen, thus adequately replicating the heat loss characteristics of the reactive mixture. The non-reactive experiment is performed under the same conditions as the corresponding reactive case, and the resulting pressure trace is converted to an “effective volume” history. The volume-time profile is then used as input for the CHEMKIN-PRO [27] closed homogeneous batch reactor module, which is used to model the experiments.

3. Results and discussion

Figures 6–14 show comparisons between model simulations and experimental data for all mixtures. Uncertainties in the ignition delay times obtained in this study are estimated as $\pm 15\%$, and are represented in the figures with error bars. In these figures, solid symbols represent experimental data obtained in the TAMU shock tube, half-filled symbols represent experiments taken in the NUIG shock tube, and open symbols represent RCM experiments. Solid lines on the graphs correspond to IDTs calculated via constant-volume, adiabatic simulations. Dashed lines represent IDTs calculated using effective volume histories from the RCM to account for facility effects. For the shock-tube experiments, a pressure rise of approximately 4% per millisecond was observed for the undiluted fuel-air experiments, while a dP/dt of 2% per ms or less was observed in the mixtures highly diluted in argon. However, for the IDTs investigated here inclusion of this pressure rise (i.e., 4% per ms) in simulations of the experiments scarcely affects numerical results. The magnitude of these effects on simulated IDTs under similar conditions to those investigated here is well illustrated in Fig. 16 of Ref. [28].

There is good agreement observed between model-simulated and experimentally obtained IDTs throughout the study. The updated and extended chemical kinetic model captures the general trends in reactivity of these fuel mixtures as functions of temperature (T), pressure (p), and equivalence ratio (ϕ). In the next sections, the effects of T , p , and ϕ on ignition delay times are discussed. This discussion will be followed by a detailed analysis of the model, the development of which is described in detail elsewhere [14]. The model presented herein differs from the one presented in Ref. [14], in that, contemporaneous to this study, there have been updates to C₀, C₂ and C₄ portions of the sub-mechanism. Specifically, within the H₂-O₂ sub-mechanism, rate coefficients from the study of Hong *et al.* [29] have been adopted for the reactions $\dot{O}H + H\dot{O}_2 \rightleftharpoons H_2O + O_2$ and $H\dot{O}_2 + H\dot{O}_2 \rightleftharpoons H_2O_2 + O_2$, along with the rate coefficient for $\ddot{O} + H_2O \rightleftharpoons \dot{O}H + \dot{O}H$ as determined theoretically by Nguyen *et al.* [30]. Several rate coefficients for reactions on the vinyl radical + O₂ potential energy surface have been adopted from the recent high-level theoretical study by Goldsmith *et al.* [31]. Extensive updates to the 2-methylpropene sub-mechanism have been carried out at NUI Galway recently, and also form part of the current sub-mechanism [32]. These updates have had minimal effects on simulated IDTs, as illustrated in Figures S9 and S10 in the Supplementary material. Also included as Supplementary material are experimental data, along with CHEMKIN [27] format kinetics, thermodynamics, and transport files. CHEMKIN input files, which include effective volume-time histories for simulation of RCM experiments, are available on the internet at <http://c3.nuigalway.ie>.

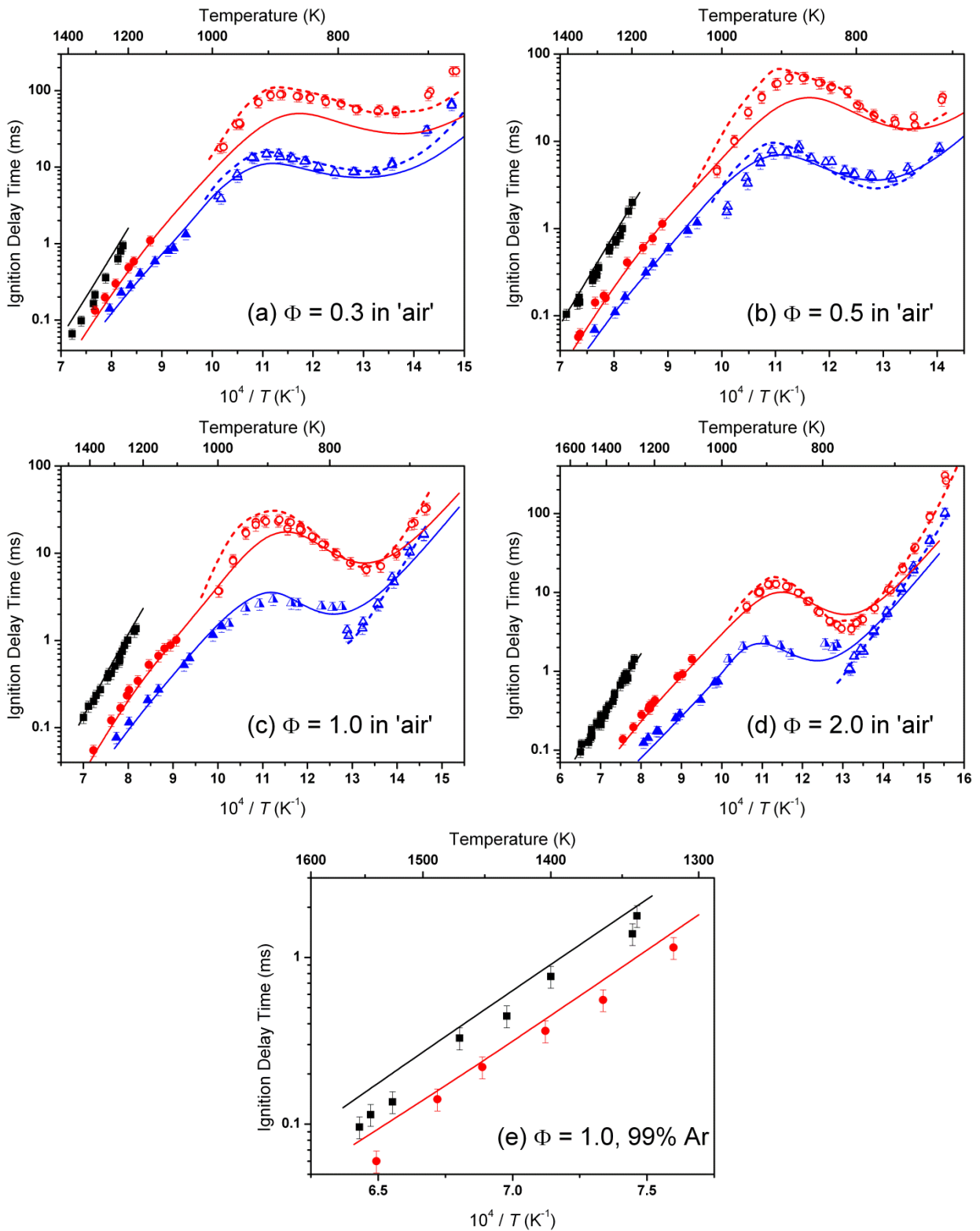


Figure 6. Effect of varying pressure on *n*-pentane reactivity. ■ – 1 atm, ● – 10 atm, ▲ – 20 atm for fuel/‘air’ (a–d) and diluted (e) mixtures. Solid symbols: TAMU ST, Half-filled symbols: NUIG ST, Open symbols: RCM. Simulation: – – RCM simulations including facility effects, — Adiabatic, constant-volume simulations.

3.1. Influence of pressure on ignition delay time

The effect of pressure on ignition delay times was studied at four different fuel/‘air’ equivalence ratios (0.3, 0.5, 1.0, and 2.0) for two of the isomers, *n*-pentane, Fig. 6, and *iso*-pentane, Fig. 7, and three different fuel/‘air’ equivalence ratios (0.5, 1.0, and 2.0) for *neo*-pentane, Fig. 8. Comparisons are also shown for each of the isomers at an equivalence ratio of 1.0 under highly dilute conditions (99% Ar). Under all conditions studied, shorter ignition delay times were measured at higher pressures. This indicates a consistent trend of increasing reactivity for all of the isomers with increasing pressure throughout this study, which is expected as reaction rate increases with concentration.

For *n*-pentane, it is shown that there is excellent agreement between the model simulated and the experimentally measured ST ignition delay times, across all temperatures, pressures, equivalence ratios, and dilutions, Fig. 6. The only noteworthy discrepancies between the model and the ST data are for the NUIG ST ignition delay times in the temperature range 778–796 K, at $\phi = 2.0$ in ‘air’, where the model simulated IDTs are shorter than those measured experimentally by ~30%.

For the RCM data below 750 K, reactivity is over-predicted by the model at fuel-lean conditions ($\phi = 0.3$ and 0.5 in ‘air’), with simulated IDTs shorter than those measured experimentally by ~30%. However, for stoichiometric and fuel-rich conditions ($\phi = 1.0$ and 2.0 in ‘air’), far better agreement is observed, with an average difference of <10% in this temperature range, at $p_C = 10$ and 20 atm.

In the negative temperature coefficient (NTC) region (~750–900 K), there is very good agreement for all investigated conditions, with average agreement between model simulations and experiments being under 10%. Reactivity is consistently under-predicted above 900 K for the RCM data.

For *iso*-pentane, Fig. 7, there is excellent agreement between the model simulations and the experimental ST data at 10 and 20 atm, where model simulated IDTs are on average approximately 10% shorter than those measured experimentally in this pressure range. However, agreement is less favourable for the 1-atm data, where model predictions are longer than experiments by approximately 30%. This disagreement is especially prevalent above 1350 K for the $\phi = 0.3$ fuel/‘air’ mixtures. However, the 1-atm dilute data show favourable agreement up to ~1580 K.

There is very good agreement between the model and the RCM experiments below 750 K for all of the conditions investigated, with average agreement being under 15%. Agreement between the model simulations and experiments in the NTC region is very favorable, within 10% for both 10 and 20 atm. As is the case with *n*-pentane, reactivity is under-predicted for RCM experiments at temperatures over 900 K.

Agreement between the ST data and model simulated IDTs for *neo*-pentane, Fig. 8, is favorable overall, but discrepancies do exist. There is good agreement between experiments and model simulations for all of the fuel/‘air’ data. However, IDTs are over-predicted by the model at the highly dilute conditions. Moreover, there is excellent agreement between experiments and model simulations for the RCM data, with average agreement being under 15% across all temperatures and pressures investigated for *neo*-pentane.

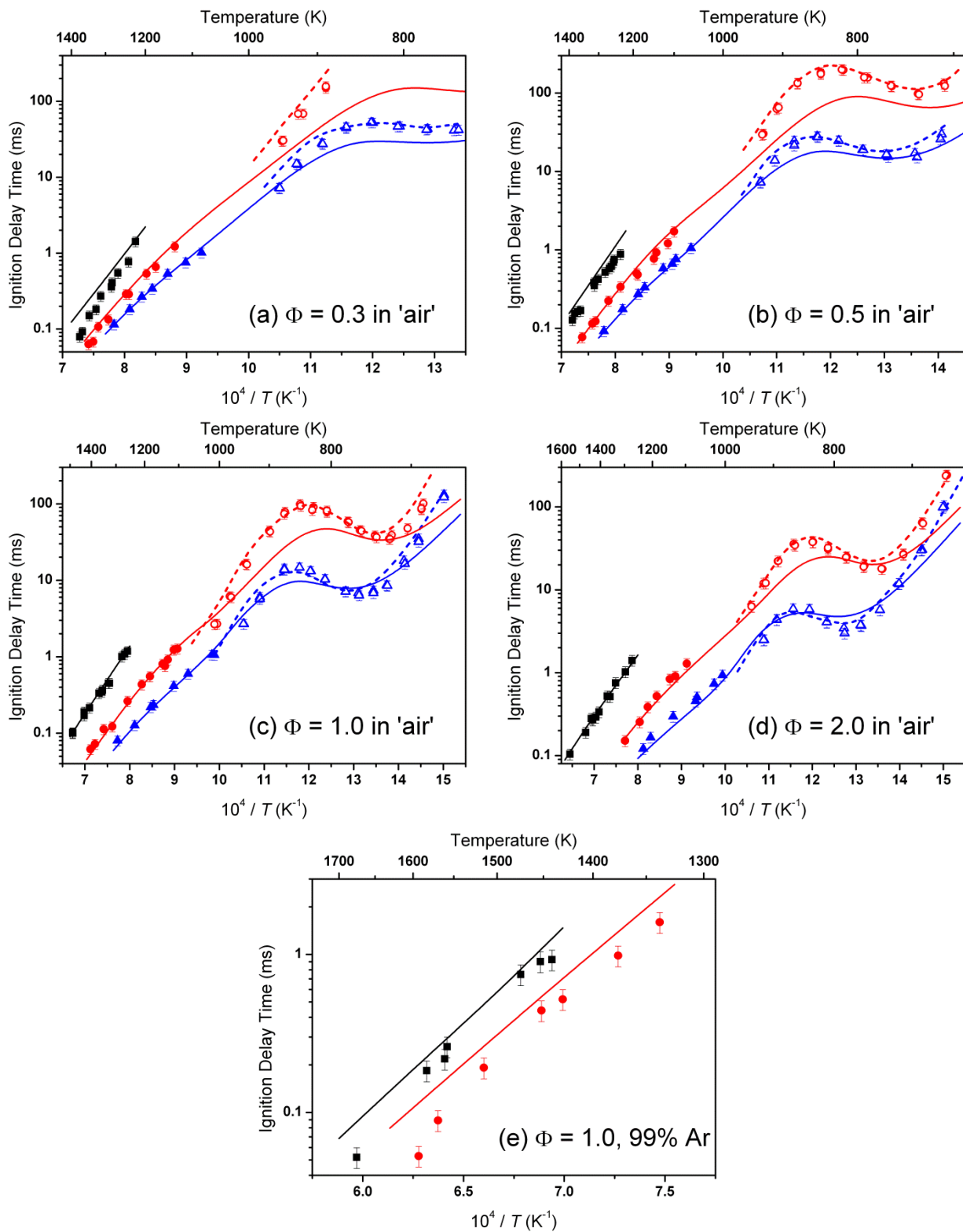


Figure 7. Effect of varying pressure on iso-pentane reactivity. ■ – 1 atm, ● – 10 atm, ▲ – 20 atm for fuel/'air' (a-d) and diluted (e) mixtures. Solid symbols: TAMU ST, Open symbols: RCM. Simulation: - - - RCM simulations including facility effects, — Adiabatic, constant-volume simulations.

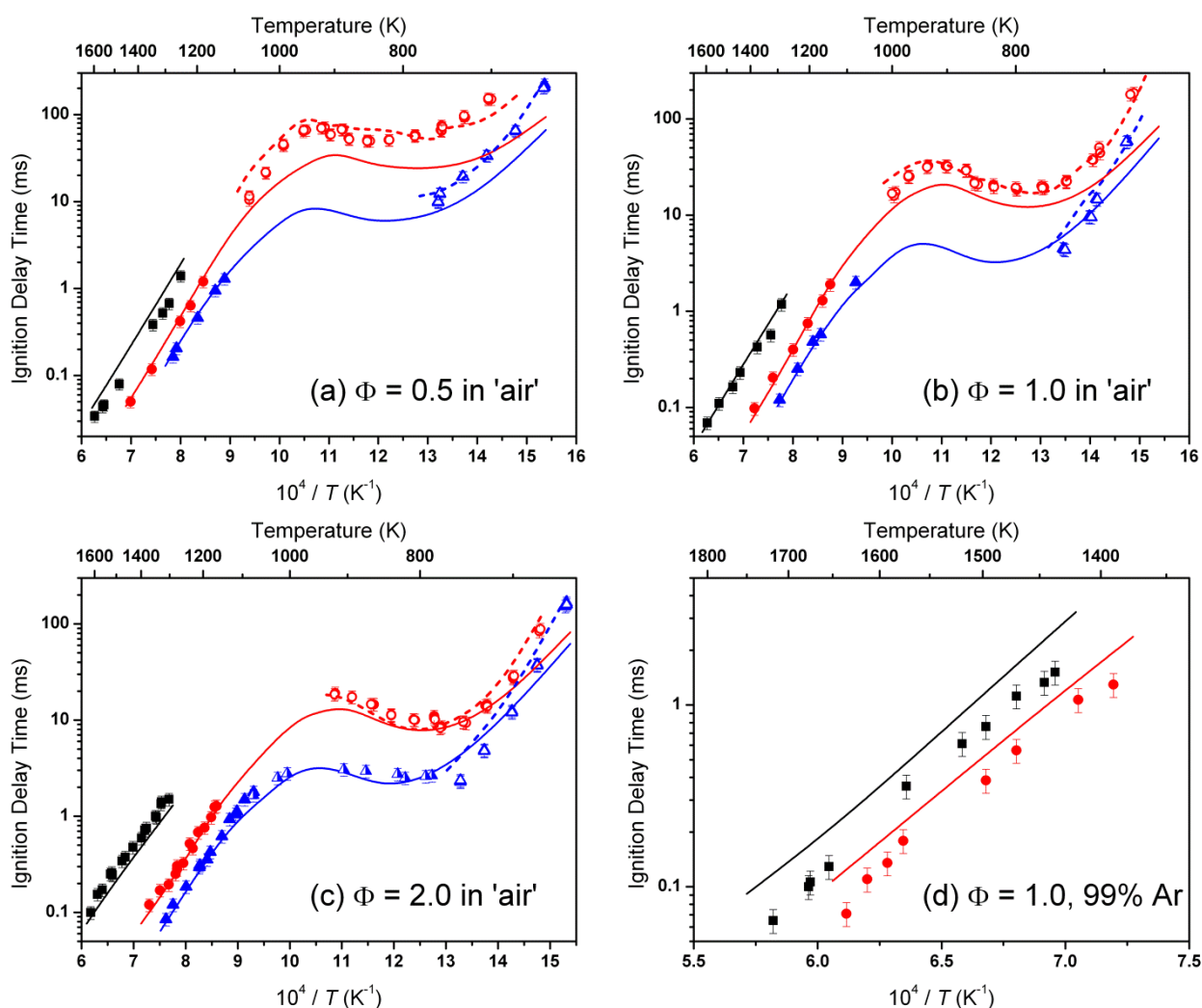


Figure 8. Effect of varying pressure on *neo*-pentane reactivity. ■ – 1 atm, ● – 10 atm, ▲ – 20 atm for fuel/‘air’ mixtures. Solid symbols: TAMU ST, Half-filled symbols: NUIG ST, Open symbols: RCM. Simulation: – – RCM simulations including facility effects, — Adiabatic, constant-volume simulations.

3.2. Influence of equivalence ratio on ignition delay time

The effect of equivalence ratio on ignition delay times was determined for four fuel/‘air’ mixture compositions at 1, 10, and 20 atm, Figs. 9–10, for *n*- and *iso*-pentane, and for three fuel/‘air’ mixture compositions at the same pressures for *neo*-pentane, Fig. 11. At low to intermediate temperatures (~650–1200 K, depending on pressure) fuel-rich mixtures ignite faster than fuel-lean ones. This behavior at low temperatures is due to an increased concentration of reactants, but more importantly an increase in fuel concentration, as the chemistry of the fuel radicals dominates and has the largest effect on ignition delay times. At intermediate temperatures, this behavior is also attributed to the fuel chemistry but is also due to the chain branching sequence $\text{RH} + \text{H}\dot{\text{O}}_2 \rightleftharpoons \dot{\text{R}} + \text{H}_2\text{O}_2$ followed by $\text{H}_2\text{O}_2 (+\text{M}) \rightleftharpoons \dot{\text{O}}\text{H} + \dot{\text{O}}\text{H} (+\text{M})$, where RH is the fuel component. Increasing the fuel concentration enhances the rate of this branching sequence that produces two reactive $\dot{\text{O}}\text{H}$ radicals. The experimental behavior at low temperatures is well captured for each of the isomers by the model.

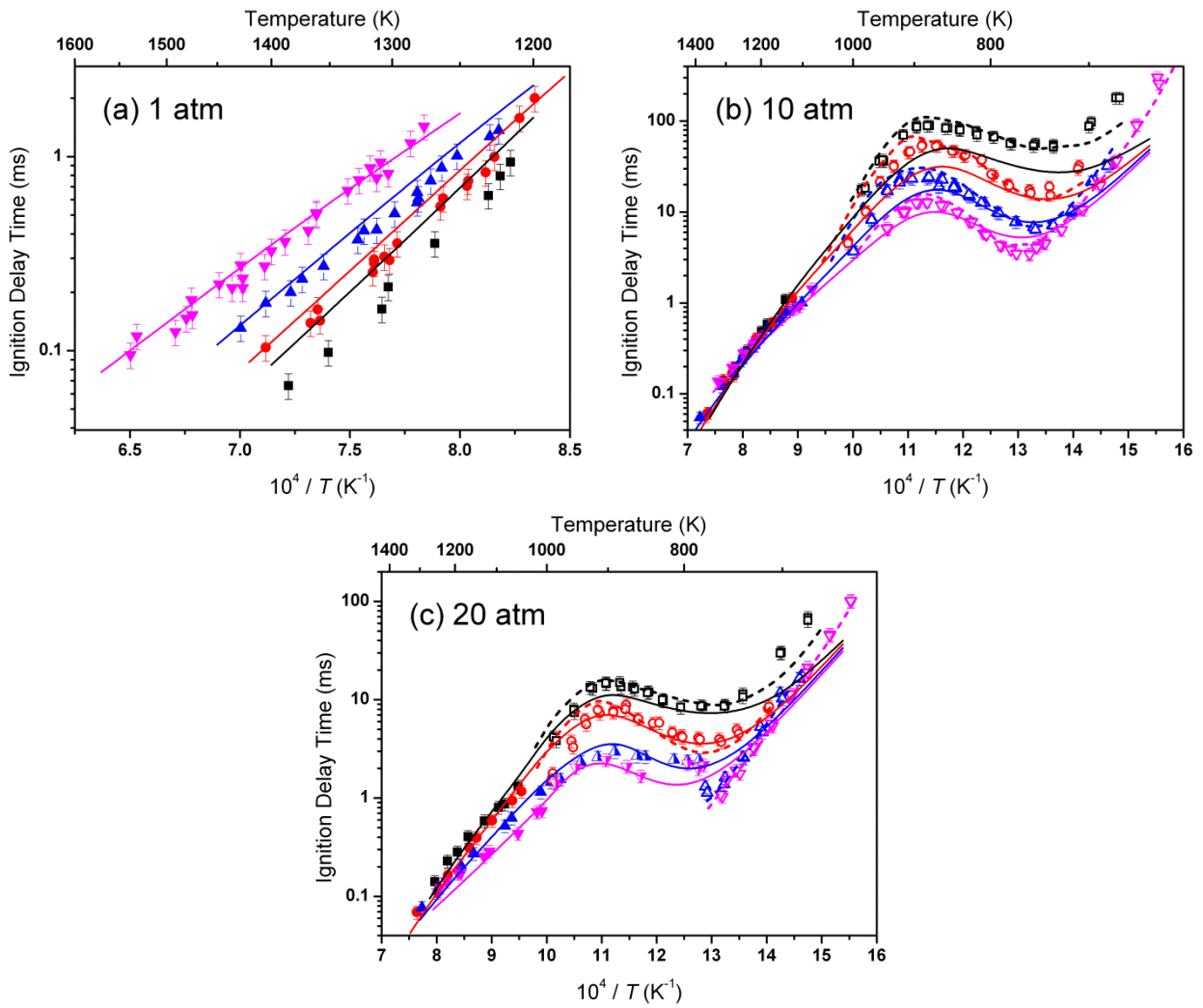


Figure 9. Effect of varying equivalence ratio (ϕ) on *n*-pentane (in 'air') reactivity. ■ – $\phi = 0.3$, ● – $\phi = 0.5$, ▲ – $\phi = 1.0$, ▼ – $\phi = 2.0$. Solid symbols: TAMU ST, Half-filled symbols: NUIG ST, Open symbols: RCM. Simulation; – – – RCM simulations including facility effects, — Adiabatic, constant-volume simulations.

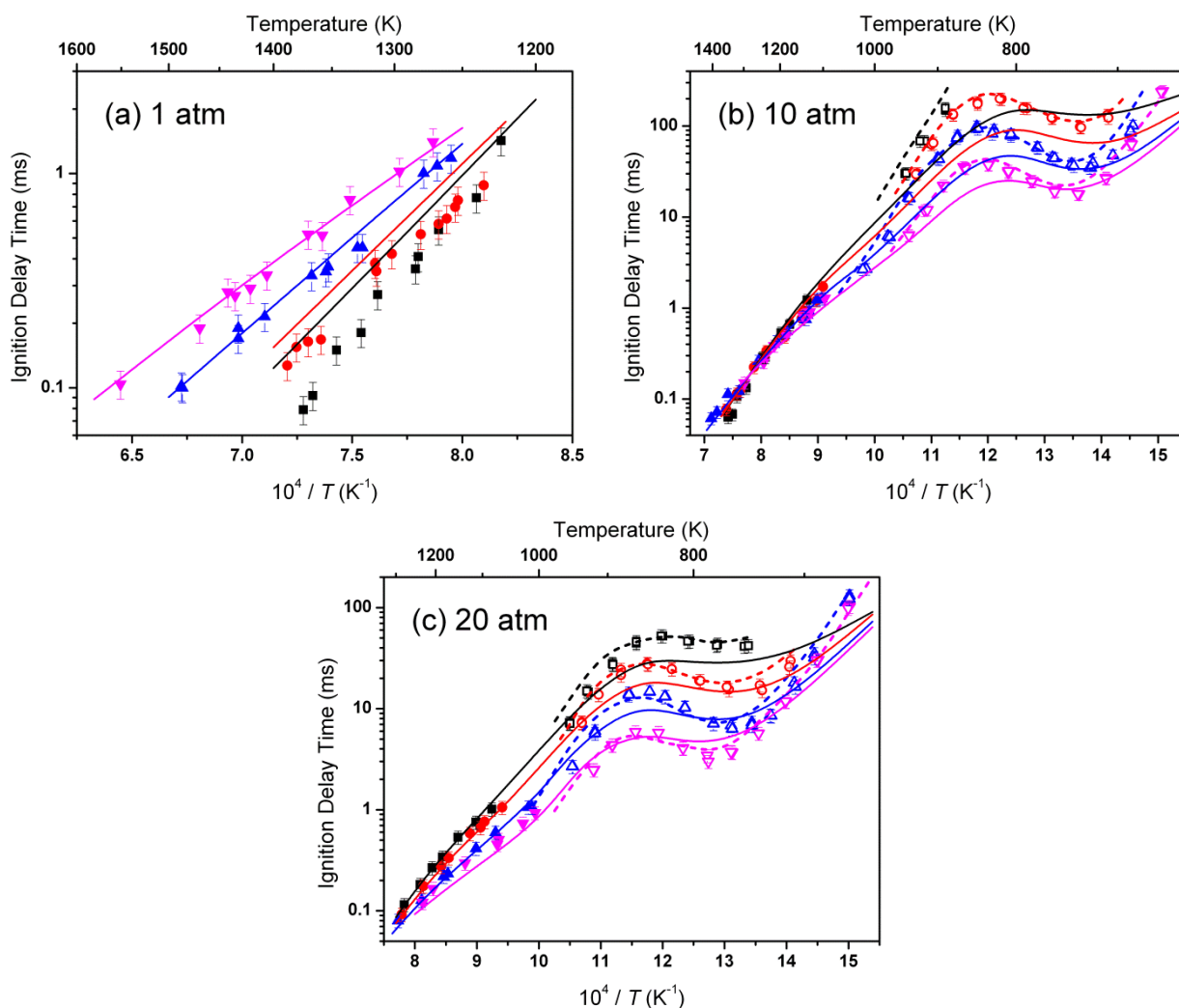


Figure 10. Effect of varying equivalence ratio (ϕ) on *iso*-pentane (in ‘air’) reactivity. ■ – $\phi = 0.3$, ● – $\phi = 0.5$, ▲ – $\phi = 1.0$, ▼ – $\phi = 2.0$. Solid symbols: TAMU ST, Open symbols: RCM. Simulation; – – RCM simulations including facility effects, — Adiabatic, constant-volume simulations.

The difference in IDTs between the mixtures is much smaller at high temperatures (1050–1400 K) relative to that at low and intermediate temperatures. However, based on the relative slopes of the data, all datasets would appear to converge at the lowest temperatures studied for 1 atm experiments, Fig. 9(a), 10(a), and 11(a). Convergence of the ignition delay times for the 10 atm cases occurs at approximately 1250 K for each of the isomers. Judging by the relative slopes of each dataset at 20 atm, it appears that the data will converge at a higher temperature than is achievable in this study due to the short ignition delay times observed in the experiments. The convergence is due to the increasing importance of the chain branching reaction $\dot{\text{H}} + \text{O}_2 \rightleftharpoons \ddot{\text{O}} + \dot{\text{O}}\text{H}$ at higher temperatures. Reaction of the fuel with H-atoms ($\text{RH} + \dot{\text{H}} \rightleftharpoons \dot{\text{R}} + \text{H}_2$) competes with the branching reaction for $\dot{\text{H}}$ atoms at higher temperatures. The fuel concentration $[\text{RH}]$ increases with increasing equivalence ratio (ϕ), so the reaction $\text{RH} + \dot{\text{H}}$ competes more effectively for $\dot{\text{H}}$ atoms at higher ϕ , and leads to longer ignition delay times. This effect of equivalence ratio is the opposite of that seen at low and intermediate temperatures.

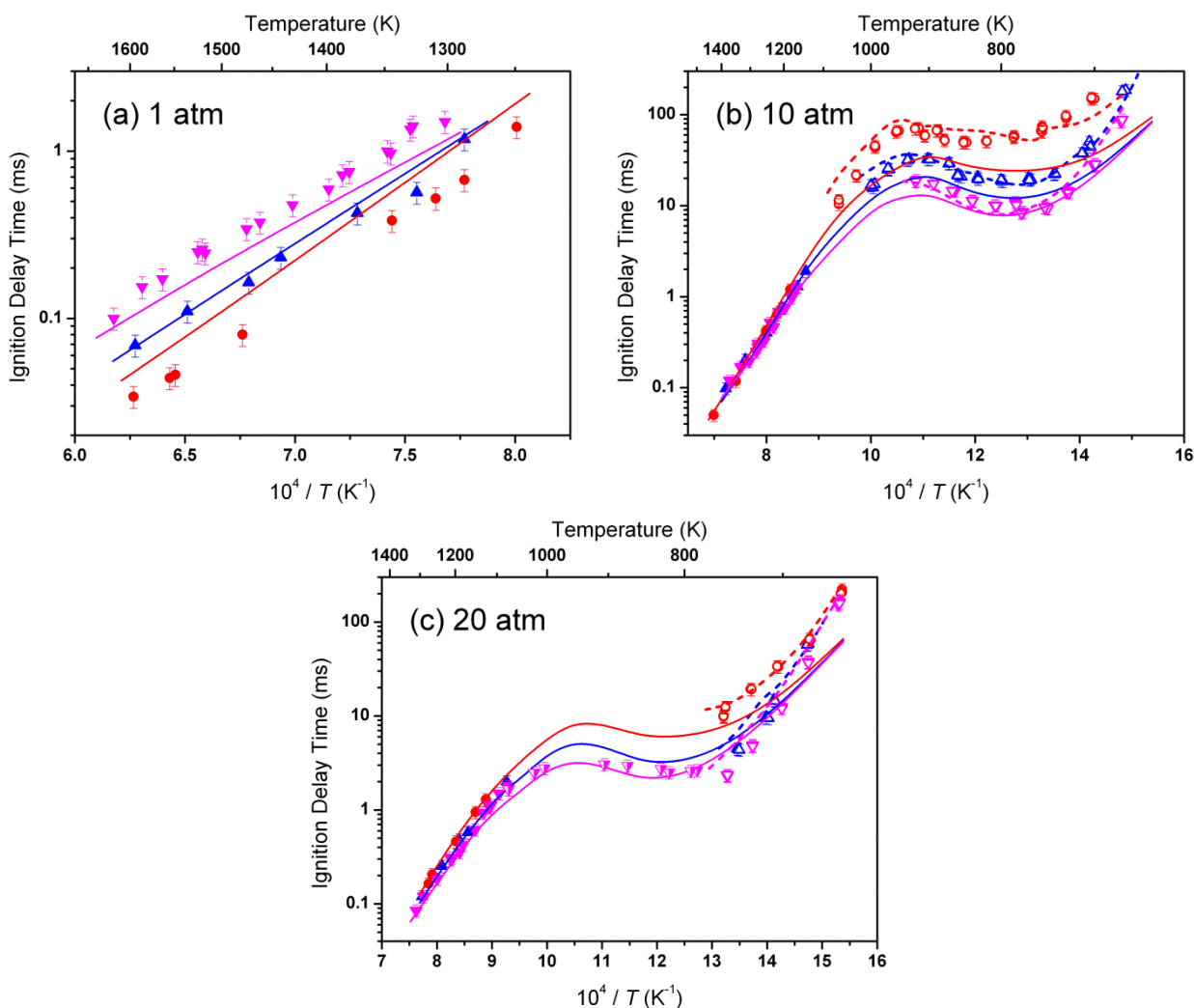


Figure 11. Effect of varying equivalence ratio (ϕ) on *neo*-pentane (in ‘air’) reactivity. ● – $\phi = 0.5$, ▲ – $\phi = 1.0$, ▼ – $\phi = 2.0$. Solid symbols: TAMU ST, Half-filled symbols: NUIG ST, Open symbols: RCM. Simulation; – – – RCM simulations including facility effects, — Adiabatic, constant-volume simulations.

3.3. Influence of fuel structure on ignition delay time

The effect of fuel structure on ignition delay times was studied at pressures of 1, 10, and 20 atm, and at equivalence ratios of 0.3, 0.5, 1.0, and 2.0 in ‘air’. Figures 12–14 show ignition delay times at the different equivalence ratios at a given pressure.

It is shown that *n*-pentane is more reactive than *iso*-pentane up to 950 K at all pressures and equivalence ratios, and exhibits similar reactivity at higher temperatures. Figures 12–14 show that *neo*-pentane is more reactive than *iso*-pentane, and less reactive than *n*-pentane at temperatures below 900 K. At these lower temperatures, *neo*-pentane shows a much less pronounced NTC region than both of the other isomers. This less-pronounced NTC behavior is due to the lack of a concerted elimination pathway for the alkyl-peroxy radical. It is the lack of this pathway that also causes *neo*-pentane to be less reactive than the other isomers at temperatures above 900 K, due to fewer hydroperoxy radicals being formed. These effects are discussed in more detail in the following sections.

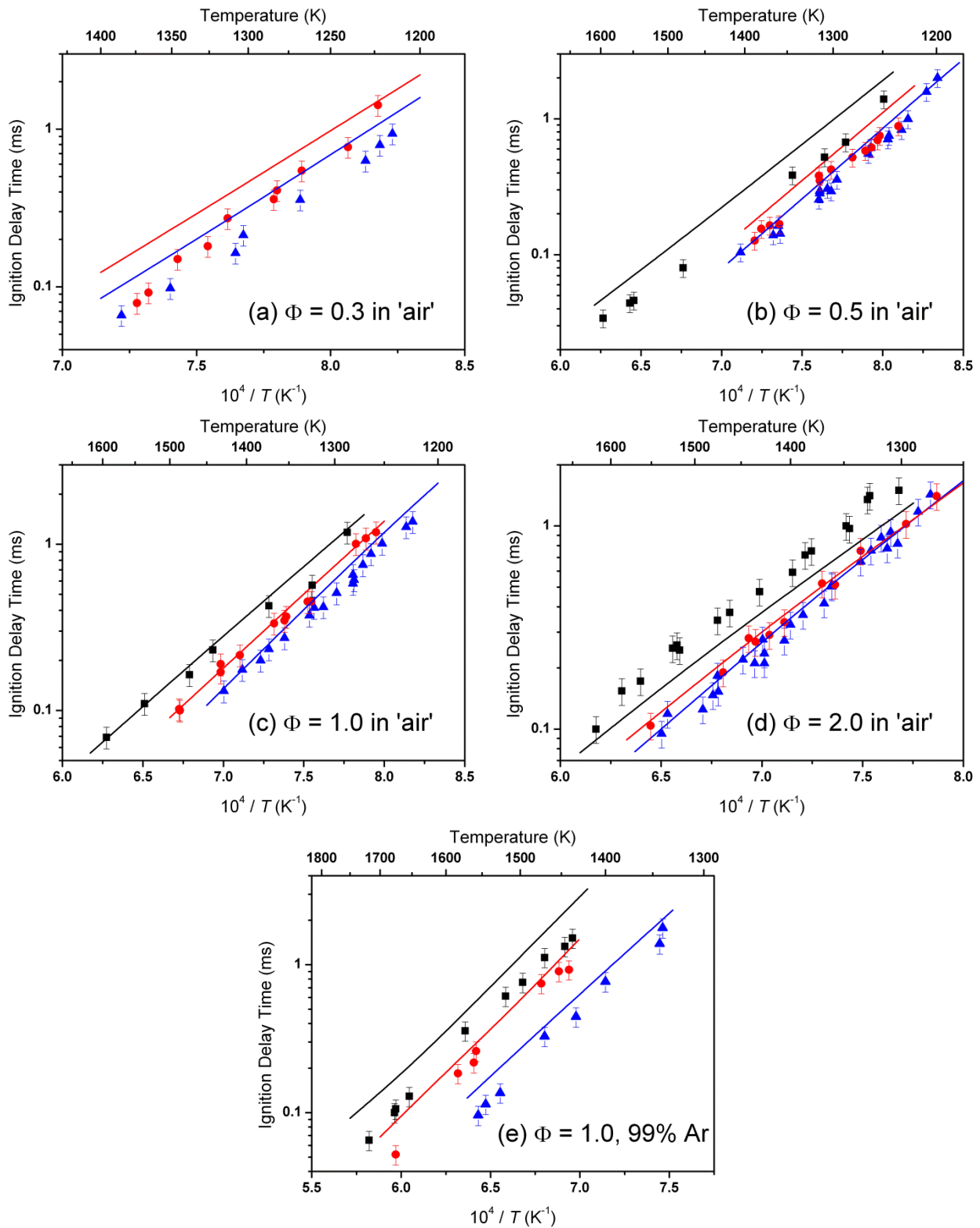


Figure 12. Effect of fuel structure on reactivity at 1 atm. \blacksquare – neo-pentane , \bullet – iso-pentane, \blacktriangle – n-pentane. Solid symbols: TAMU ST. Simulation; — Adiabatic, constant-volume simulations.

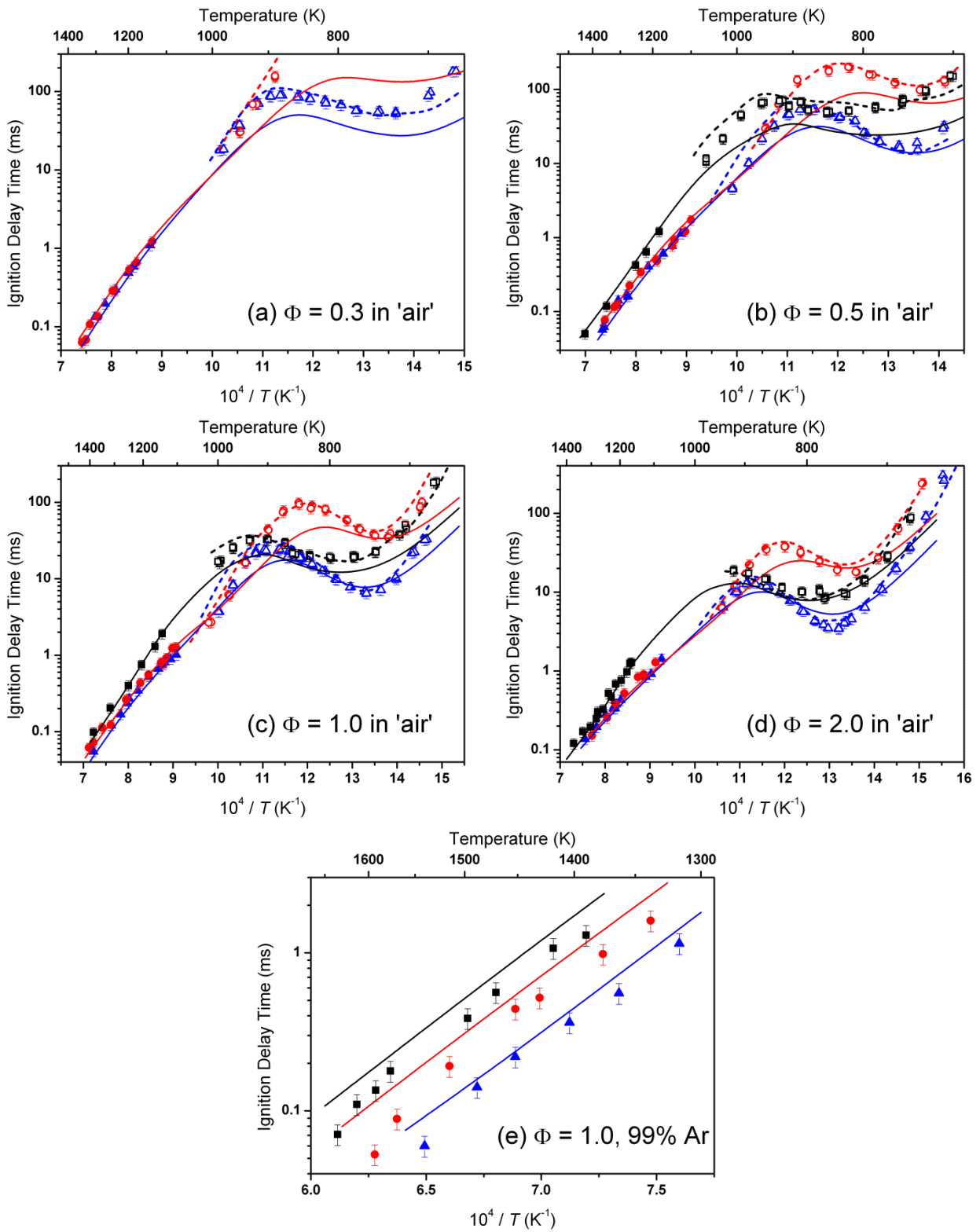


Figure 13. Effect of fuel structure on reactivity at 10 atm. ■ – *neo*-pentane , ● – *iso*-pentane, ▲ – *n*-pentane. Solid symbols: TAMU ST, Open symbols: RCM. Simulation; – – RCM simulations including facility effects, — Adiabatic, constant-volume simulations.

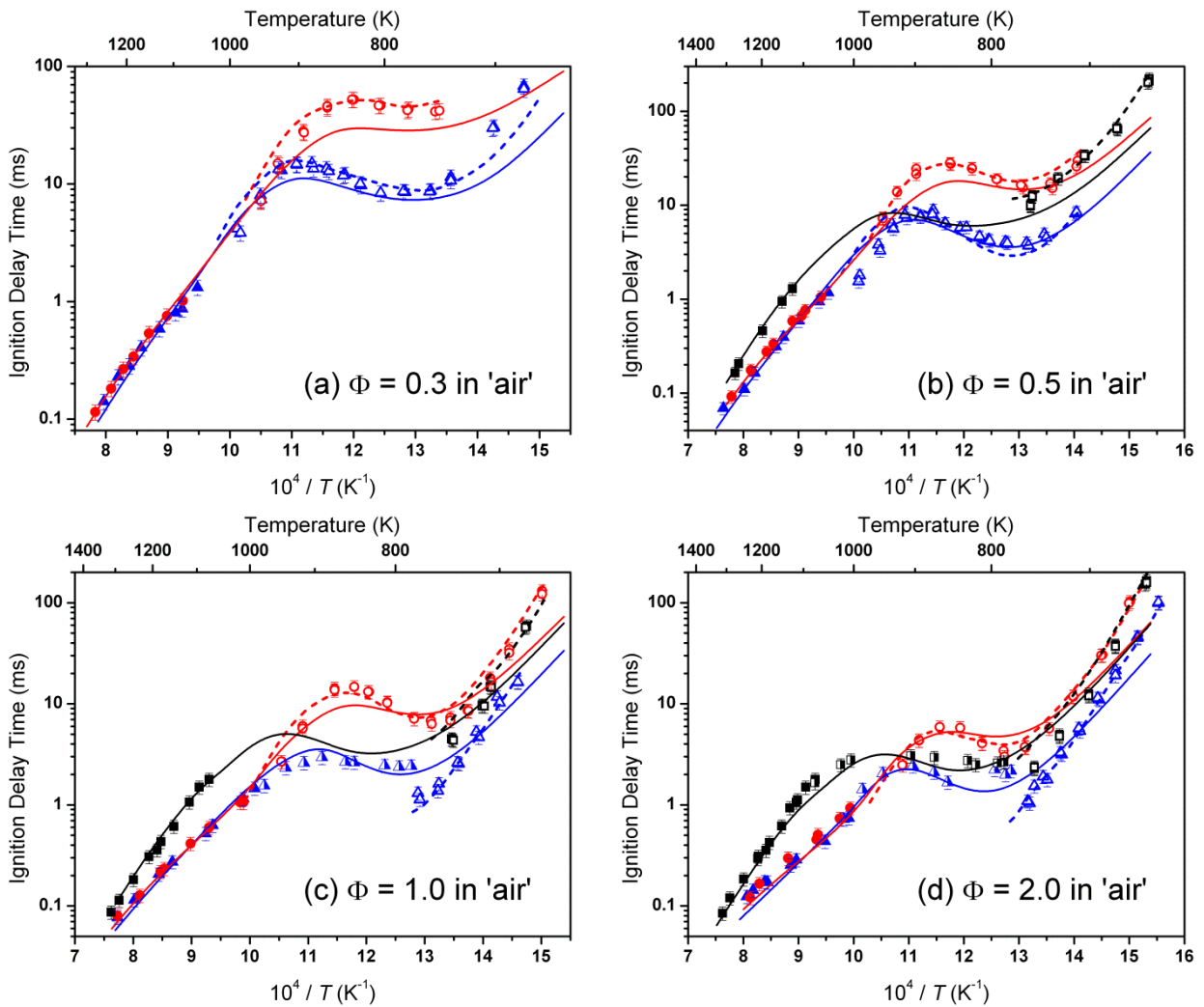


Figure 14. Effect of fuel structure on reactivity at 20 atm. ■ – neo-pentane , ● – iso-pentane, ▲ – n-pentane. Solid symbols: TAMU ST, Half-filled symbols: NUIG ST, Open symbols: RCM. Simulation; – – – RCM simulations including facility effects, — Adiabatic, constant volume simulations.

3.4. Flux analyses

Flux analyses were carried out at $\phi = 1.0$ in 'air' and 10 atm for a series of temperatures (750 K, 950 K, 1150 K, and 1350 K) and at 20% fuel consumed, these being most representative for the experimental conditions studied.

These flux analyses cover the most common reactions occurring at various temperature regimes, Figs. 15–17. For brevity, any reaction paths representing <5% flux have been excluded from Figs. 15–17.

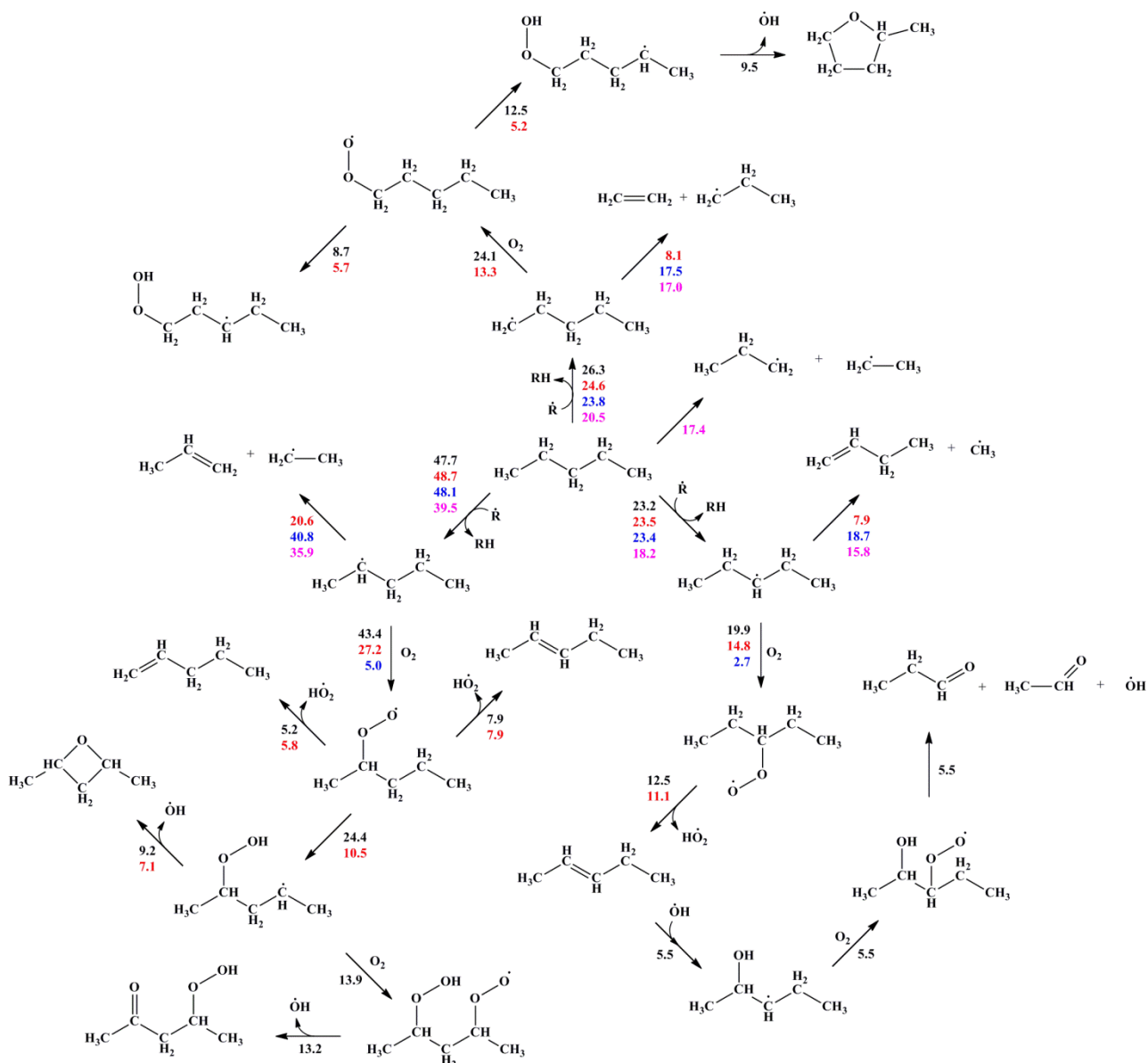


Figure 15. Flux analysis carried out for *n*-pentane oxidation at $\phi = 1.0$ in ‘air’, 10 atm and 20% fuel consumption. Numbers represent the percentage of fuel flux that goes through a particular species. Black numbers represent flux at 750 K, red numbers represent flux at 950 K, blue numbers represent flux at 1150 K, and magenta numbers represent flux at 1350 K. \dot{R} is the sum of \dot{OH} , \dot{HO}_2 and \dot{CH}_3 radicals and \dot{H} and \dot{O} atoms.

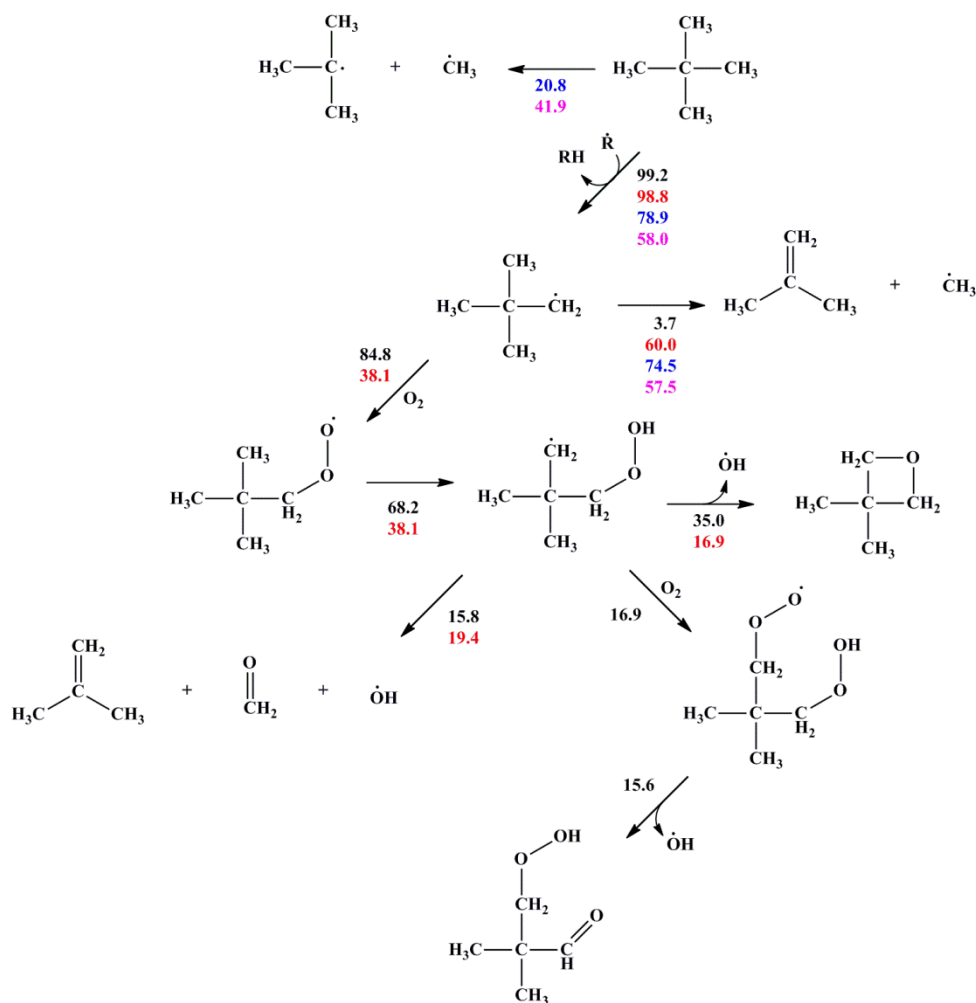


Figure 17. Flux analysis carried out for *neo*-pentane oxidation at $\phi = 1.0$ in ‘air’, 10 atm and 20% fuel consumption. Numbers represent the percent of fuel flux that goes through a particular species. Black numbers represent flux at 750 K, red numbers represent flux at 950 K, blue numbers represent flux at 1150 K, and magenta numbers represent flux at 1350 K. \dot{R} is the sum of $\dot{O}H$, $\dot{H}O_2$ and $\dot{C}H_3$ radicals and \dot{H} and \dot{O} atoms.

For each of the isomers at 750 K (numbers in black font, Fig. 15–17), the fuel is completely consumed via H-atom abstraction by $\dot{O}H$, $\dot{H}O_2$, and $\dot{C}H_3$ radicals and \dot{H} and \dot{O} atoms. Of these radicals, $\dot{O}H$ accounts for >90% of the consumption of each of the fuels at this temperature. The main reaction pathway (>80%) for the resulting fuel radicals is addition to O_2 . At this point, the majority of the fuel molecules for each of the isomers have progressed through pathways resulting in the formation of alkyl-peroxy radicals ($R\dot{O}_2$), with little variation amongst the fuels. However, there are significant differences amongst the isomers regarding the competition between the main consumption pathways of the $R\dot{O}_2$ radicals.

For *n*- and *iso*-pentane, the main pathways for $R\dot{O}_2$ radical reactions are: (i) isomerization to form hydroperoxyl-alkyl radicals ($\dot{Q}OOH$), and (ii) concerted elimination reactions forming an olefin and a hydroperoxyl radical. This competition plays an important role in the low-temperature oxidation of these fuels. The production of a $\dot{Q}OOH$ radical may lead to chain branching reactions, which increases reactivity by forming hydroxyl radicals. Concerted elimination reactions curtail the progression towards chain branching pathways and result in the production of less reactive hydroperoxyl radicals.

Figure 15 shows that H-atom abstraction from two of the three equivalent sites on *n*-pentane results in the major pathway leading to the formation of a $\dot{Q}OOH$ radical, with abstraction from the third site leading mostly to the formation of an olefin and a hydroperoxyl radical. Similarly, in Fig. 16 it is shown that H-atom abstraction from the two primary sites on *iso*-pentane mainly leads to a $\dot{Q}OOH$ radical, with abstraction from the other two sites (secondary and tertiary) leading to an olefin and a hydroperoxyl radical. A simple investigation of the flux analyses, such as this, provides an explanation for the difference observed in reactivity between the two fuels, Figs. 13 and 14.

Similarly, a flux analysis of *neo*-pentane at 750 K shows that the main pathway for RO_2 radical consumption results in the formation of $\dot{Q}OOH$ radicals. There is only one equivalent abstraction site on *neo*-pentane, and the concerted elimination pathway is not possible from the RO_2 radical which is eventually formed, because there is no C–H bond beta to the peroxy moiety. Due to the lack of a concerted elimination pathway, it is expected that fuel reactivity would be enhanced. This result is true when compared to *iso*-pentane, Fig. 13 and 14. The NTC region is also much less pronounced for *neo*-pentane compared to the other two isomers, due to the higher ratio of chain branching to chain propagating pathways, brought about by the lack of a concerted elimination pathway. The reason for *neo*-pentane not being more reactive compared to *n*-pentane at 750 K is that it has less facile options to progression towards chain branching reactions due to the absence of secondary C–H bonds, which are weaker than primary C–H bonds, which *n*-pentane contains. The relative abundance of secondary C–H bonds on *n*-pentane allows for faster isomerization reactions of alkyl-peroxy radicals, and subsequently permits faster $\dot{Q}OOH$ radical additions to molecular oxygen, which lead to chain branching.

At 950 K, there is a shift towards chain propagating pathways for all of the fuels. A higher proportion of the fuel radicals undergo β -scission reactions to form an olefin and a small alkyl radical, rather than adding to molecular oxygen. For *n*- and *iso*-pentane, in the competition between the main consumption pathways of RO_2 radicals the concerted elimination reactions are favored. Cyclic ether formation and β -scission reactions of $\dot{Q}OOH$ radicals are dominant over addition to molecular oxygen for each of the isomers at this temperature.

We see that the majority of the fuel molecules decompose to smaller species at 1150 K for all of the isomers, mainly via H-atom abstraction, followed by β -scission of the fuel radical. For *neo*-pentane, it is shown that uni-molecular decomposition of the fuel to produce a *tert*-butyl and a methyl radical plays a significant role at this temperature.

For each of the isomers, the fuel decomposes almost entirely via two classes of reaction pathways at 1350 K. The main consumption pathways involve H-atom abstraction, followed by β -scission of the fuel radical, as observed at 1150 K. The remaining fuel molecules mostly decompose via uni-molecular decomposition of the parent fuel molecule, producing two small alkyl radicals. Again, at this temperature, there is little variation between the decomposition pathways of the isomers.

3.5. Sensitivity analyses

Using CHEMKIN-PRO [27], brute force sensitivity analyses of different reaction rate coefficients were computed at 750 K, 950 K, 1150 K, and 1350 K at 10 atm and $\phi = 1.0$ in ‘air’, for each of the isomers. The analyses were performed by increasing and decreasing the rate coefficients by a factor of two, with sensitivities expressed using the formula:

$$\sigma = \frac{\log_{10}(\tau_+/\tau_-)}{\log_{10}(k_+/k_-)} = \frac{\log_{10}(\tau_+/\tau_-)}{\log_{10}(2/0.5)}$$

where σ is the sensitivity coefficient, τ_+ is the simulated IDT when a given rate coefficient is multiplied by a factor of two, τ_- is the simulated IDT when a given rate coefficient is divided by a factor of two, and k_+ and k_- are the factors by which the rate coefficients have been multiplied. A positive sensitivity coefficient indicates a reaction that will increase simulated ignition delay times if the rate coefficient for that reaction is increased. Conversely, a negative sensitivity coefficient relates to a reaction that will decrease simulated ignition delay times if the rate coefficient for that reaction is increased. This analysis was carried out for all of the reactions in the mechanisms.

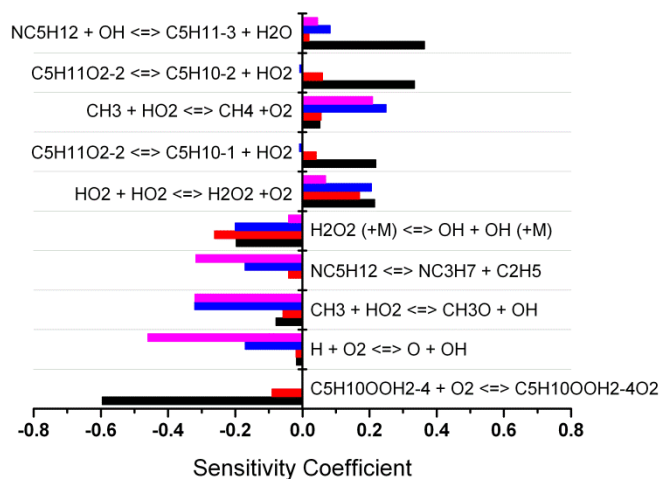


Figure 18. Sensitivity analyses for *n*-pentane, $\phi = 1.0$ in ‘air’, $p = 10$ atm, at $T =$ ■ 750 K, ■ 950 K, ■ 1150 K, and ■ 1350 K.

Figure 18 shows that the reaction classes of major importance to *n*-pentane oxidation at 750 K are H-atom abstractions by $\dot{\text{O}}\text{H}$ radicals, concerted eliminations of $\text{H}\dot{\text{O}}_2$ from $\text{R}\dot{\text{O}}_2$ radicals, and $\dot{\text{Q}}\text{OOH}$ radical addition to O_2 . H-atom abstractions from the fuel producing 1- and 2-pentyl radicals promote reactivity, and in Fig. 15 it is shown that some of the main consumption pathways of these radicals result in chain branching, with the production of two hydroxyl radicals. The hydroxyl radicals are highly reactive, and lead to fuel consumption. $\dot{\text{Q}}\text{OOH}$ radical addition to O_2 forms part of this chain of reactions, hence the high sensitivity coefficient for the reaction of this type in Fig. 14. H-atom abstractions from the central carbon on *n*-pentane, producing 3-pentyl radicals, greatly inhibit reactivity at this temperature. Figure 15 shows that the major consumption pathway of 3-pentyl radicals results in chain propagation, with hydroperoxyl radicals produced via concerted elimination from the alkyl-peroxyl radicals which are formed upon addition of 3-pentyl radicals to molecular oxygen. It is shown in Fig. 18 that these concerted elimination reactions are highly inhibiting at this temperature. One of the reasons for this is that the $\dot{\text{O}}\text{H}$ radical producing pathways (most importantly, the chain branching pathways proceeding via carbonyl-hydroperoxide species) are cut off. Another reason is that the $\text{H}\dot{\text{O}}_2$ radicals that are produced are far less reactive than the $\dot{\text{O}}\text{H}$ radicals that would have otherwise been formed, and H-atom abstraction reactions by hydroperoxyl radicals are far more endothermic than those of hydroxyl radicals.

At 950 K, there is a shift in the order of importance of reactions classes to those involving H_2O_2 chemistry. At this temperature, H_2O_2 can overcome the relatively high barrier for uni-molecular decomposition to form two highly reactive hydroxyl radicals, $\text{H}_2\text{O}_2 (+\text{M}) \rightleftharpoons \dot{\text{O}}\text{H} + \dot{\text{O}}\text{H} (+\text{M})$. This

step highly promotes reactivity because the main consumption pathways of the fuel are H-atom abstractions by $\dot{\text{O}}\text{H}$ radicals. The main production pathways of H_2O_2 at this temperature are $\text{H}\dot{\text{O}}_2 + \text{H}\dot{\text{O}}_2 \rightleftharpoons \text{H}_2\text{O}_2 + \text{O}_2$, and H-atom abstraction from *n*-pentane by $\text{H}\dot{\text{O}}_2$ radicals. The all-important hydroperoxyl radicals are mainly produced via concerted elimination reactions from alkyl-peroxyl radicals. Figure 18 shows that reaction of two hydroperoxyl radicals with one another to form hydrogen peroxide and molecular oxygen inhibits reactivity. This behavior is somewhat counterintuitive because the hydrogen peroxide produced from this reaction mostly decomposes to produce two hydroxyl radicals, which highly promotes reactivity. However, this reaction competes with the other major consumption pathway of $\text{H}\dot{\text{O}}_2$ radicals, which is H-atom abstraction from the fuel. If both hydroperoxyl radicals were to instead abstract from the fuel, two hydrogen peroxide molecules would be formed, which can decompose to form four hydroxyl radicals.

At 1150 K, reactions of H_2O_2 and $\text{H}\dot{\text{O}}_2$ radicals are still of relative importance. Alongside these reactions, the fate of methyl radicals plays an important role. Figure 18 shows that $\dot{\text{C}}\text{H}_3 + \text{H}\dot{\text{O}}_2 \rightleftharpoons \text{CH}_4 + \text{O}_2$ inhibits reactivity at this temperature. This reaction competes with $\dot{\text{C}}\text{H}_3 + \dot{\text{C}}\text{H}_3 (+\text{M}) \rightleftharpoons \text{C}_2\text{H}_6 (+\text{M})$ and $\dot{\text{C}}\text{H}_3 + \text{H}\dot{\text{O}}_2 \rightleftharpoons \text{CH}_3\dot{\text{O}} + \dot{\text{O}}\text{H}$. The reaction of methyl and hydroperoxyl radicals to form methane and molecular oxygen, and the methyl-methyl recombination reaction, both inhibit reactivity, as two radicals react to produce two stable products in both cases. However, the reaction of methyl and hydroperoxyl radicals to form methoxy and hydroxyl radicals is highly promoting. The main consumption pathways of the fuel molecules are H-atom abstractions by $\dot{\text{O}}\text{H}$. This is one of the reasons why the reaction $\dot{\text{C}}\text{H}_3 + \text{H}\dot{\text{O}}_2 \rightleftharpoons \text{CH}_3\dot{\text{O}} + \dot{\text{O}}\text{H}$ promotes reactivity. The other is that the methoxy radical which is produced mainly decomposes via β -scission to form formaldehyde and a H-atom. The H-atoms which are produced can react via $\dot{\text{H}} + \text{O}_2 \rightleftharpoons \dot{\text{O}} + \dot{\text{O}}\text{H}$. This reaction also promotes reactivity at this temperature, Fig. 14, and is highly branching, and dominates reactivity at 1350 K.

Hydrogen atoms are mostly produced via β -scission of ethyl radicals. The majority of ethyl radicals come from two main pathways: (i) uni-molecular decomposition of *n*-pentane to produce *n*-propyl and ethyl radicals, and (ii) β -scission of 2-pentyl radical to produce *n*-propyl and ethyl radicals. The reaction of $\dot{\text{H}}$ atoms with O_2 promotes reactivity so much because it is a chain branching reaction, with one radical in the reactants, and two in the products. But also, the main reaction pathway for both oxygen atoms and hydroxyl radicals is H-atom abstraction from the fuel. These reactions are highly exothermic, and the $\dot{\text{O}}\text{H}$ radicals produced from the reaction of $\dot{\text{O}}$ atoms with *n*-pentane will go on to abstract from another fuel molecule. Overall, due to reaction of hydrogen atoms with molecular oxygen, three highly reactive radicals are effectively created, with each one undergoing a subsequent, highly exothermic reaction.

The most sensitive reactions for both *iso*- and *neo*-pentane oxidation are very similar to those for *n*-pentane. Therefore, descriptions of their sensitivity analyses will be succinct, as the important reaction pathways have been discussed in detail for *n*-pentane.

The most sensitive reactions for *iso*-pentane at 750 K include H-atom abstractions by $\dot{\text{O}}\text{H}$ radicals, and concerted eliminations of $\text{H}\dot{\text{O}}_2$ from $\text{R}\dot{\text{O}}_2$ radicals, Fig. 19. H-atom abstractions from the primary carbon sites highly promote reactivity, whereas abstractions from the secondary and tertiary sites greatly inhibit reactivity.

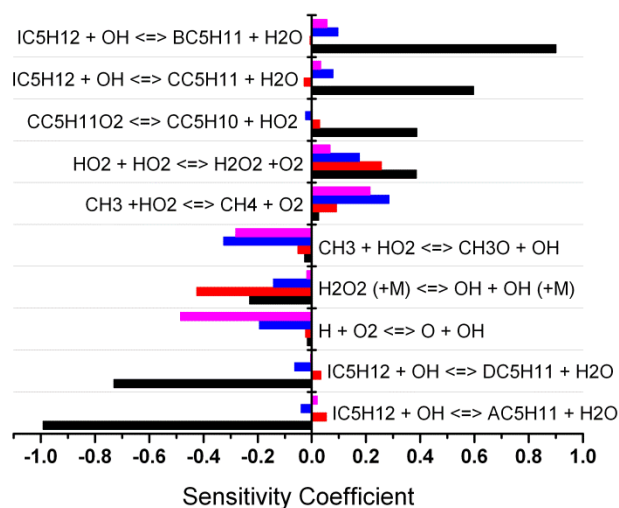


Figure 19. Sensitivity analyses for *iso*-pentane, $\phi = 1.0$ in ‘air’, $p = 10$ atm, at $T =$ ■ 750 K, ■ 950 K, ■ 1150 K, and ■ 1350 K.

2-methyl-but-1-yl ($\dot{A}C_5H_{11}$), 2-methyl-but-2-yl ($\dot{B}C_5H_{11}$), 3-methyl-but-2-yl ($\dot{C}C_5H_{11}$) and 3-methyl-but-1-yl ($\dot{D}C_5H_{11}$) radicals are the four distinct radicals which can be formed from *iso*-pentane. It is shown in Fig. 16 that the primary fuel radicals have a higher percentage flux through pathways leading to chain branching reactions. This result is in contrast to the other two fuel radicals, which mainly react through concerted elimination pathways.

At 950 K, $\dot{H}O_2/H_2O_2$ chemistry plays an important role in controlling reactivity. The two major H_2O_2 production pathways ($\dot{H}O_2 + \dot{H}O_2 \rightleftharpoons H_2O_2 + O_2$, and H-atom abstractions from the fuel by $\dot{H}O_2$ radicals) show large coefficients in the sensitivity analysis for *iso*-pentane at this temperature, Fig. 19.

Chemistry pertaining to small radical species becomes more prominent at 1150 and 1350 K. The branching ratios of the consumption pathways of hydroperoxyl and methyl radicals are all-important, alongside the branching reaction of \dot{H} atoms and molecular oxygen, with the latter dominating reactivity at 1350 K.

As is the case with the other two isomers, H-atom abstraction reactions from *neo*-pentane by $\dot{O}H$ radicals, and hydroperoxyl *neo*-pentyl ($\dot{Q}OOH$) radical addition to O_2 show high sensitivity at 750 K, Fig. 20. This is because both of these reactions aid progression towards chain branching reactions which proceed via formation and decomposition of carbonyl-hydroperoxide species. At higher temperatures, similar trends are observed for *neo*-pentane as were discussed earlier for *n*- and *iso*-pentane. The chemistry of hydroperoxyl and methyl radicals and that of \dot{H} atoms via the reaction $\dot{H} + O_2 \rightleftharpoons \dot{O} + \dot{O}H$ becomes increasingly important.

Thus far, the reaction pathways of each of the isomers have been analysed in detail. Focusing on low temperatures (~ 600 – 900 K), where NTC behavior is observed, it is seen that the pathways controlling reactivity involve $\dot{R}O_2$ and $\dot{Q}OOH$ radicals, and the competition between chain branching and chain propagating reactions. While our understanding of what causes NTC behavior (i.e. chain branching versus chain propagating) is further corroborated by this study, an interesting point arises. While it is often postulated that dissociation of $\dot{R}O_2$ radicals producing fuel radicals and O_2 contributes to NTC behavior, we find no evidence here to support this claim.

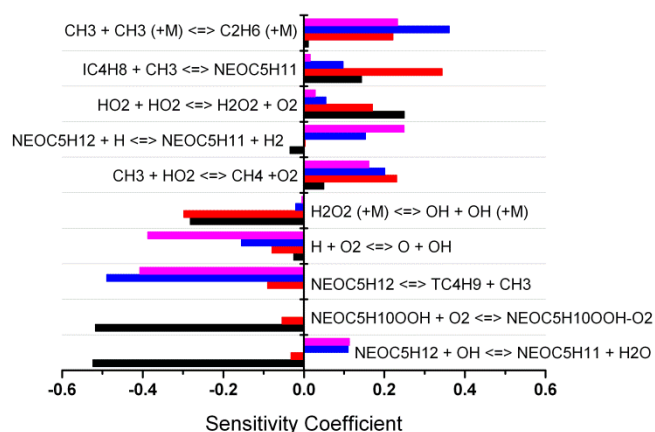


Figure 20. Sensitivity analyses for *neo*-pentane, $\phi = 1.0$ in ‘air’, $p = 10$ atm, at $T =$ ■ 750 K, ■ 950 K, ■ 1150 K, and ■ 1350 K.

A simple test of making addition reactions of fuel radicals to O_2 irreversible (i.e. not allowing back-dissociation of $\dot{R}O_2$) shows that not only does NTC behavior persist, but simulated IDTs decrease by a negligible amount in the case of *n*- and *iso*-pentane, and while the effect is more pronounced for *neo*-pentane, it still exhibits NTC behavior. Therefore, the $\dot{R} + O_2 \rightleftharpoons \dot{R}O_2$ equilibrium is not controlling NTC behavior. The reason for the more pronounced effect on *neo*-pentane is due to its unusual structure and symmetry, which results in the back-dissociation pathway being one of only two important reactions that the *neo*-pentylperoxyl radical participates in; the other being isomerization to hydroperoxyl *neo*-pentyl radical. This is in contrast to the over 20 important reactions which *n*-pentylperoxyl and *iso*-pentylperoxyl radicals undergo. Illustrations of these effects are shown in Figures S11 and S12 in the Supplementary material. While it may be intuitive that the back-dissociation pathway would play a major role, the reality is that the depth of the potential energy well ($\sim 35\text{--}38$ kcal mol $^{-1}$) upon addition of fuel radicals to O_2 relative to the barrier heights of the subsequent reactions of $\dot{R}O_2$ radicals, ensures that the dissociation pathway is only of minor importance. The important equilibrium is that of $\dot{R}O_2 \rightleftharpoons \dot{Q}OOH$ radicals, with the important competition being mainly between the concerted elimination reactions of $\dot{R}O_2$ radicals, and the addition of $\dot{Q}OOH$ radicals to O_2 . The former pathway is a chain propagation reaction and cuts off the chain of reactions which could otherwise lead to chain branching, while the $\dot{Q}OOH$ radical addition to O_2 mostly leads to chain branching.

4. Conclusions

This study presented a comprehensive experimental and modelling study of the shock tube and rapid compression machine ignition of the pentane isomers over a temperature range of 643–1718 K, equivalence ratios of 0.3, 0.5, 1.0 and 2.0 in ‘air’, and reflected shock/compressed pressures of 1, 10 and 20 atm, and highly dilute (99% argon) mixtures at stoichiometric conditions and reflected shock pressures near 1 and 10 atm.

The influence of pressure on IDTs is as expected, with an increase in reflected shock/compressed pressure resulting in shorter ignition delay times at a given temperature. This trend is observed for all equivalence ratios investigated. The effect of equivalence ratio is also as expected, with fuel rich mixtures having shorter IDTs than fuel lean mixtures throughout the lower and intermediate temperature ranges. However, at higher temperatures the IDTs converge, and cross over at the lower pressures investigated herein.

Ignition delay times calculated using the model developed as part of this study show good agreement with the experimentally measured IDTs, thus validating the model for homogeneous ignition. The experimental data also provide important insights into trends in reactivity in terms of temperature, pressure, equivalence ratio, dilution, and fuel structure.

This study, in conjunction with its partner study [27], provides a significant contribution to the understanding of the oxidation of the simplest type of hydrocarbons; alkanes. Extensive changes to thermochemistry and kinetics of species and reaction pathways important at low temperatures have provided a solid base from which to construct larger mechanisms, be they alkane oxidation mechanisms or otherwise. It remains to be seen if such an overhaul of model parameter values will be necessary for previously proposed biofuel/oxygenated fuel models, such as the butanol isomers, given that many thermochemical and rate parameters therein are derived by analogy with alkanes.

While there have been significant strides in recent years in furthering the understanding of low-temperature oxidation, a more concerted effort is required if such strides are to be made in the future.

Acknowledgments

NUI Galway would like to acknowledge the support of the Irish Research Council in funding this work. The TAMU efforts were funded in part by Rolls-Royce Canada under the direction of Dr. Gilles Bourque; the TEES Turbomachinery Laboratory; and the National Science Foundation under grant number EEC-1004859.

References

- [1] C. K. Westbrook, H. J. Curran, W. J. Pitz, J. F. Griffiths, C. Mohamed, S. K. Wo, The Effects of Pressure, Temperature, and Concentration on the Reactivity of Alkanes: Experiments and Modeling in a Rapid Compression Machine, *Proc. Combust. Inst.* 27 (1) (1998) 371–378.
- [2] M. Ribaucour, R. Minetti, L. R. Sochet, H. J. Curran, W. J. Pitz, C. K. Westbrook, Ignition of Isomers of Pentane: An Experimental and Kinetic Modeling Study, *Proc. Combust. Inst.* 28 (2) (2000) 1671–1678.
- [3] R. Minetti, A. Roubaud, E. Therssen, M. Ribaucour, L. R. Sochet, The Chemistry of Pre-Ignition of *n*-Pentane and 1-Pentene, *Combust. Flame* 118 (1–2) (1999) 213–220.
- [4] R. Minetti, M. Ribaucour, M. Carlier, L. R. Sochet, Autoignition Delays of a Series of Linear and Branched Chain Alkanes in the Intermediate Range of Temperature, *Combust. Sci. Tech.* 113 (1) (1996) 179–192.
- [5] D. B. Dahm, F. H. Verhoek, McPherson Chemical Laboratory, The Ohio State University, Columbus, Ohio 43210 (1968).
- [6] A. Burcat, K. Scheller, A. Lifshitz, Shock-Tube Investigation of Comparative Ignition Delay Times for C₁–C₅ Alkanes, *Combust. Flame* 16 (1) (1971) 29–33.
- [7] V. P. Zhukov, V. A. Sechenov, A. Yu. Starikovskii, Self-Ignition of a Lean Mixture of *n*-Pentane and Air over a Wide Range of Pressures, *Combust. Flame* 140 (3) (2005) 196–203.
- [8] C. K. Westbrook, W. J. Pitz, M. M. Thornton, P. C. Malte, A Kinetic Modeling Study of *n*-Pentane Oxidation in a Well-Stirred Reactor, *Combust. Flame* 72 (1) (1998) 45–62.
- [9] F. S. Gonzalez, S. Sandler, An Experimental Study of the Oxidation of *n*-Pentane in the High Temperature Pre-Ignition Region, *Combust. Flame* 26 (1976) 35–44.
- [10] M. A. Oehlschlaeger, D. F. Davidson, J. T. Herbon, R. K. Hanson, Shock Tube Measurements of Branched Alkane Ignition Times and OH Concentration Time Histories, *Int. J. Chem. Kinet.* 36 (2) (2004) 67–78.
- [11] S. Wang, D. L. Miller, N. P. Cernansky, H. J. Curran, W. J. Pitz, C. K. Westbrook, A Flow Reactor Study of Neopentane Oxidation at 8 Atmospheres: Experiments and Modeling, *Combust. Flame* 118 (3) (1999) 415–430.
- [12] D. Healy, D. M. Kalitan, C. J. Aul, E. L. Petersen, G. Bourque, H. J. Curran, Oxidation of C₁–C₅ Alkane Quinary Natural Gas Mixtures at High Pressures, *Energy Fuels* 24 (2010) 1521–1528.
- [13] H. J. Curran, P. Gaffuri, W. J. Pitz, C. K. Westbrook, A Comprehensive Modeling Study of *iso*-Octane Oxidation, *Combust. Flame* 129 (3) (2002) 253–280.
- [14] J. Bugler, K. P. Somers, E. J. Silke, H. J. Curran, Revisiting the Kinetics and Thermodynamics of the Low-Temperature Oxidation Pathways of Alkanes: A Case Study of the Three Pentane Isomers, *J. Phys. Chem. A* 119 (28) (2015) 7510–7527.

- [15] C. J. Aul, W. K. Metcalfe, S. M. Burke, H. J. Curran, E. L. Petersen, Ignition and Kinetic Modeling of Methane and Ethane Fuel Blends with Oxygen: A Design of Experiments Approach, *Combust. Flame* 160 (2013) 1153–1167.
- [16] R. Mével, P. A. Boettcher, J. E. Shepherd, Absorption Cross Section at 3.39 μm of Alkanes, Aromatics and Substituted Hydrocarbons, *Chem. Phys. Lett.* 531 (2012) 22–27.
- [17] A. E. Klingbeil, J. B. Jeffries, R.K. Hanson, Temperature- and Pressure-Dependent Absorption Cross Sections of Gaseous Hydrocarbons at 3.39 μm , *Meas. Sci. Technol.* 17 (2006) 1950–1957.
- [18] E. L. Petersen, Interpreting Endwall and Sidewall Measurements in Shock-Tube Ignition Studies, *Combust. Sci. Technol.* 181 (2009) 1123–1144.
- [19] D. Darcy, C. J. Tobin, K. Yasunaga, J. M. Simmie, J. Würmel, W. K. Metcalfe, T. Niass, S. S. Ahmed, C. K. Westbrook, H. J. Curran, A High Pressure Shock Tube Study of *n*-Propylbenzene Oxidation and its Comparison with *n*-Butylbenzene, *Combust. Flame* 159 (7) (2012) 2219–2232.
- [20] W. S. Affleck, A. Thomas, An Opposed Piston Rapid Compression Machine for Pre-Flame Reaction Studies, *Proc. Inst. Mech. Eng.* 183 (1968) 365–387.
- [21] L. Brett, J. MacNamara, P. Musch, J. M. Simmie, Simulation of Methane Autoignition in a Rapid Compression Machine with Creviced Pistons, *Combust. Flame* 124 (2001) 326–329.
- [22] D. Lee, S. Hochgreb, Rapid Compression Machines: Heat Transfer and Suppression of Corner Vortex, *Combust. Flame* 114 (1998) 531–545.
- [23] D. Lee, S. Hochgreb, Hydrogen Autoignition at Pressures above the Second Explosion Limit (0.6–4.0 MPa), *Int. J. Chem. Kinet.* 30 (1998) 385–406.
- [24] J. Würmel, J. M. Simmie, CFD Studies of a Twin-Piston Rapid Compression Machine, *Combust. Flame* 141 (4) (2005) 417–430.
- [25] C. Morley, *GasEq, Version 0.76*, <http://www.gaseq.co.uk> (2004).
- [26] D. Darcy, H. Nakamura, C. J. Tobin, M. Mehl, W. K. Metcalfe, W. J. Pitz, C. K. Westbrook, H. J. Curran, A High-Pressure Rapid Compression Machine Study of *n*-Propylbenzene Ignition, *Combust. Flame* 161 (1) (2014) 65–74.
- [27] CHEMKIN-PRO 15101, Reaction Design, San Diego, 2010.
- [28] K. P. Somers, J. M. Simmie, F. Gillespie, C. Conroy, G. Black, W. K. Metcalfe, F. Battin-Leclerc, P. Dirrenberger, O. Herbinet, P.-A. Glaude, P. Dagaut, C. Togbé, K. Yasunaga, R. X. Fernandes, C. Lee, R. Tripathi, H. J. Curran, A Comprehensive Experimental and Detailed Chemical Kinetic Modelling Study of 2,5-Dimethylfuran Pyrolysis and Oxidation, *Combust. Flame* 160 (2013) 2291–2318.
- [29] Z. Hong, K. -Y. Lam, R. Sur, S. Wang, D. F. Davidson, R. K. Hanson, On the Rate Constants of $\text{OH} + \text{HO}_2$ and $\text{HO}_2 + \text{HO}_2$: A Comprehensive Study of H_2O_2 Thermal Decomposition using Multi-Species Laser Absorption, *Proc. Combust. Inst.* 34 (1) (2013) 565–571.

- [30] T. L. Nguyen, J. F. Stanton, Ab Initio Thermal Rate Calculations of $\text{HO} + \text{HO} = \text{O}(^3\text{P}) + \text{H}_2\text{O}$ Reaction and Isotopologues, *J. Phys. Chem. A* 117 (13) (2013) 2678–2686.
- [31] C. F. Goldsmith, L. B. Harding, Y. Georgievskii, J. A. Miller, S. J. Klippenstein, Temperature and Pressure-Dependent Rate Coefficients for the Reaction of Vinyl Radical with Molecular Oxygen, *J. Phys. Chem. A* 119 (28) (2015) 7766–7779.
- [32] C.-W. Zhou, Y. Li, E. O'Connor, K. P. Somers, S. Thion, E. L. Petersen, T. A. DeVerter, M. A. Oehlschlaeger, G. Kukkadapu, C. -J. Sung, M. Alrefae, F. Khaled, A. Farooq, P. Dirrenberger, P.-A. Glaude, F. Battin-Leclerc, J. Santner, Y. Ju, H. J. Curran, Comprehensive Experimental and Modeling Study of Isobutene Oxidation, in preparation.